Underwater Acoustic MIMO OFDM: An experimental analysis

Guillem Palou
Advisor: Milica Stojanovic
Massachusetts Institute of Technology

September 2009

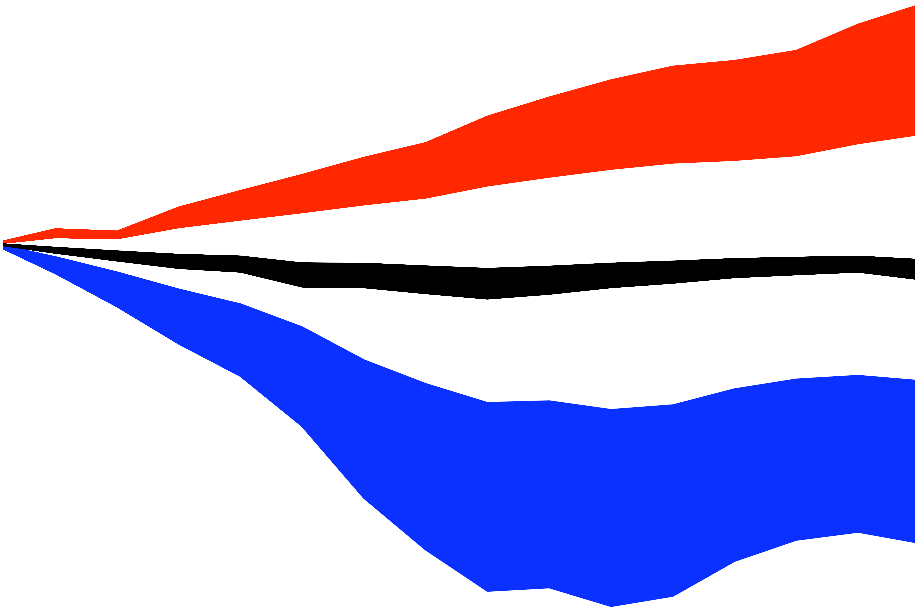

Contents

List of Figures

Acknowledgements

I first would like to thank people who helped me to be able to do this work. Milica, as my advisor, helped me in all the problems and sugggestions I had. Her open mind showed me how to look at the problems in many different ways, and try to solve them by seeking another perspective. I'm also thankful to MIT, specially the Sea Grant College, who offered me a lab and treated me like all the others in the team. My labmates in MIT, Jordi, Willy, Thang and Roman, were wonderful persons to share work with. Nevertheless, regular meetings at Northeastern University, made the work more interesting, being able to learn from other people, namely Ashish, Parastoo, Yashar, Rameez, Francesco, Baosheng and Joao.
The work would have not be the same if life outside the laboratory didn't exist. Specially I would like to mention my roommate in the best house ever, 357 Columbia St., Jordi. Funny, intelligent and very... let's say critic. I want to mention also other spanish people who were present in my Bostonian life, Martin, Guillem, Hector, Miquel, Agua, Anna who was also my roommate; without them, I would have not been able to do it. Thanks to all.
I would like to recognize my family for the sacrifice of missing me during all these months; and specially my girlfriend Alba, with whom I spent a whole month during the summer. She was all I needed during this period of time, she knew how I felt, she knew what to do; and now that it's all over I don't know how to thank her for all her effort. At least I can put her name in this document. :)

Resum

Recentment, els esforços de recerca han provat que el Multiplexat de Divisio Ortogonal en freqüència (OFDM per les seves sigles en anglès) representa una alternativa viable a les comunicacions de portadora única, que han estat utilitzades tradicionalment per enllaços de gran *bitrate* en entorns acústics submarins. La principal atracció de l'OFDM és la seva simplicitat en els processos de modulació, demodulació, implementats via FFT/IFFT.
La recerca prèvia s'ha focalitzat en el disseny d'algorismes adaptatius que engloben totes les funcions necessàries de la capa física per un módem: sincronització (adquisició inicial i seguiment), estimació del canal (tan el mètode convencional com el dispers), detecció de les dades amb la seva corresponen decodificació. Totes aquestes característiques a més d'utilitzar diversos receptors així com més d'un transmissor per un enllaç anomenat MIMO (Multiple-Input Multiple-Output) formen l'avantguarda de la nova generació de mòdems subaquàtics.
Només recentment s'ha començat a experimentar en entorns reals. OFDM ha estat ampliament utilitzat en entorns radio, fins al punt d'estar inclòs a diversos estandards de l'IEEE. En comunicacions subaquàtiques, aquesta tècnica de multiplexat en frequència és recent com per poder tenir resultats novedosos en aquest àmbit. Donat que els primers tests experimentals van ser satisfactoris, la qüestió que es planteja ara és la dels límits de l'OFDM. L'objectiu d'aquest treball serà mesurar aquests límits i veure si tenen alguna relació amb les condicions físiques o metorològiques, analitzant un seguit d'experiments reals que van tenir lloc prop de la costa de Cape Cod.
L'efficiència d'un sistema MIMO-OFDM ve donada per $R/B = mM_T/(1 + T_gB/K)$ bps/Hz, on m es el nivell de modulació (els bits per símbol, per ser més concrets), M_T és el nombre d'elements transmissors, T_g és el temps de guarda que el sistema utilitza entre dos blocks consecutius OFDM per evitar el multipath i que ha de ser més llarg que el retard per multipropagació del canal T_{mp}, B es l'ample de banda total que s'utilitza i finalment K és el número de subportadores que generalment es una potència de 2 com ara 128, 256... 1024. Com que els sistemes acústics estan limitats per banda a causa de la gran atenuació que sofreixen les altes freqüències, si es vol augmentar l'efficiència, l'únic que es pot modificar son el número de transmissors i les subportadores. Aquests paràmetres, tanmateix, estan restringits també per la capacitat de processat i pel canal mateix. Una de les consideracions que s'assumeix en OFDM és que el canal resta invariant durant un block. Aleshores, incrementant el numero de subportadores (amb B fixe) resulta en un increment del temps de símbol OFDM ($T = K/B$), cosa que possibilita al canal variar la seva resposta durant aquest bloc. Mentre el temps de bloc estigui per sota del temps de coherència del canal no hi ha cap problema; en el moment que aquestes dues duracions son comparables, violem un dels principis d'estacionarietat de la FFT. Encara que un processat post FFT pot compensar aquesta distorsió fins a un cert punt utilitzant tècniques de cancelació de ICI (Inter-carrier Interference), una variació del canal important pot causar pèrdues irrecuperables. L'única manera de constrarestar aquest efecte

es mitjançant mètodes pre-FFT; encara que utilitzant un processat més complex redueix les avantatges de la simplicitat de l'OFDM. Així doncs, la variació temporal del canal imposa un clar límit a l'efficiència d'un sistema OFDM en el número de subportadores que es poden arribar a utilitzar.
El nombre d'elements transmissors que pot encabir un sistema està limitat per la quantitat de conversa creuada (cross-talk en anglès, efecte conegut per les les línies telefòniques analògiques) que pot suportar l'estimador de canal MIMO. És obvi que, com més cross-talk hi hagi, més díficil serà la tasca de separar la informació i així més díficil serà estimar el canal. Quantitativament, per que un receptor tingui suficients observacions per estimar M_T respostes del canal, la llargada de cada una d'elles, $L = \lceil T_{mp} B \rceil$, està limitada per la condició $M_T \leq K/L$. Això vol dir que si eventualment, donades el número de subportadores i el nombre de transmissors, L és realment més llarga que el que pot estimar el sistema, l'estimació de canal no serà del tot correcta. Així, si establim un altre cop l'equació de l'eficiència del sistema en funció de la llargada del canal, trobem que aquesta eficiència és, com a maxim, $K^2/(LK + L^2)$ símbols per segon i per Hertz.
L'anàlisi experimental que s'ha dut a terme en aquest estudi es focalitza en senyals acústiques enregistrades durant un període de 15 dies durant l'Octubre de 2008. L'experiment va ser realitzat al sud de l'illa Martha's Vineyard a Cape Cod, Massachusetts. Un sistema 4×12 MIMO va ser desplegat amb una distància entre transmissors i receptors de 1000 m en una profunditat de 15m a l'oceà Atlàntic. Les condicions de l'experiment van resultar ser molt variables, amb perídodes de gran activitat d'onades i de forts vents. Les senyals van ser transmeses en la banda de 8 a 18 kHz ($B = 10$ kHz) i diversos paràmetres van anar variant-se, incloent diferents tipus de modulació, com ara QPSK i 8-PSK, amb un rang de subportadores de 128 a 1024. Aquesta selecció de paràmetres correspon a una eficiència espectral, sense codificar, de 0.9 a 10.4 bps/Hz. Aquest ampli rang ha permès posar a prova tant el sistema com el canal per a poder arribar a conclusions fermes.
Les senyals han estat processades utilitzant un algoritme que incorpora una compensació no uniforme de l'efecte Doppler. Com que la naturalesa física del sistema fa que sigui de banda ampla, la distorsió per efecte Doppler en una freqüència que en una altra. L'estimació del canal MIMO ha estat realitzada utilitzant l'algoritme [2], el qual explota de manera òptima la coeherència del canal en el domini freqüèncial. Els resultats obtinguts revelen (a) variació del rendiment del sistema, que poden ser fins a un punt deguts també a la variació de les condicions meteorlògiques; (b) una millora del rendiment al augmentar el número de subportadores per un nombre de transmissors determinat, fet que implica que el límit imposat pel temps de coherència no ha estat assolit amb les condicions presents; d'aquesta manera s'impulsa l'estimació del canal ja que com més subportadores suporti el sistema, més observacions per una correcta estimació són disponibles. Finalment, (c) el rendiment del sistema decreix quan s'augmenta el nombre de transmissors, cosa que, per altra banda, es d'esperar degut a l'increment de *bitrate* del sistema.

Abstract

Research efforts over the past several years have provided ample proof that orthogonal frequency division multiplexing (OFDM) represents a viable alternative to single-carrier modulation which has traditionally been used for high rate communications over underwater acoustic channels. The main attraction of OFDM lies in its simplicity of implementation via FFT modulation/demodulation, which makes it a candidate for implementation in the next generation of acoustic modems.

Prior work has focused on the design and conceptual testing of adaptive detection algorithms that encompass all the necessary functions of the physical layer modem: synchronization (initial acquisition and continued tracking), channel estimation (conventional and sparse), and data detection and decoding; all in configuration with multiple receive elements, as well as a single or multiple transmit elements. With successful completion of initial field tests, a question naturally arises as to what are the limits of OFDM performance. We address this question through an experimental analysis.

Bandwidth efficiency of MIMO OFDM is given as $R/B = mM_T/(1+T_gB/K)$ bps/Hz, where m is the modulation level, M_T is the number of transmit elements, $T_g \geq T_{mp}$ is a guard time greater than the multipath spread of the channel T_{mp}, B is the total system bandwidth, and K is the number of carriers. Since acoustic systems are bandwidth-limited, pushing the OFDM performance limits rests on increasing the number of carriers and transmit elements. These parameters, however, are restricted by the capabilities of signal processing and the channel itself. Specifically, increasing the number of carriers results in an increased OFDM block duration ($T = K/B$), which in turn allows for a larger channel variation to occur over one block. The time-coherence assumption, necessary for FFT demodulation, is thus eventually violated. While a post-FFT processor can compensate for some amount of time-variation by inter-carrier interference (ICI) cancellation, a larger variation will cause an irrecoverable loss during FFT demodulation. The only way in which this can be prevented is by pre-FFT processing; however, using a more complex processor would diminish the original appeal of OFDM–its simplicity. Hence, the temporal variation of the channel imposes a fundamental limit on the number of carriers K in a conventional OFDM system.

The number of transmit elements M_T is limited by the amount of cross-talk that can be handled by a MIMO channel estimator. In particular, in order for the receiver to have a sufficient number of signal observations to estimate M_T channel responses, each of length $L = \lceil T_{mp}B \rceil$, the number of transmitters has to be $M_T \leq K/L$. Hence, the bandwidth efficiency of a MIMO OFDM system is at most $K^2/(LK + L^2)$ symbols per second per Hertz.

Our experimental analysis focuses on acoustic signals recorded over a period of 15 days during an October 2008 test conducted south of the island of Martha's Vineyard in the Atlantic Ocean. A 4×12 MIMO system was deployed over a 1 km range in about 15 m of water. The conditions during the experiment were varying, with periods of high

wave activity. The signals, transmitted in the 8-18 kHz band (B=10 kHz), included 4- and 8-PSK with varying number of carriers ranging between K=128 and 1024. This selection of signal parameters corresponds to a large range of bandwidth efficiencies, from 0.9 to 10.4 bps/Hz.

The signals were processed using an adaptive algorithm that incorporates non-uniform Doppler compensation and sparse channel estimation. MIMO channel estimation was accomplished using the algorithm [2], which optimally exploits channel coherence in the frequency domain. These results reveal (a) performance variation over the course of the experiment, which can to some extent be correlated with the environmental condition; (b) performance improvement with an increase in the number of carriers for a given number of transmit elements, which implies that the coherence limit is not reached within the present conditions, thus boosting the decision-directed channel estimation by increasing the number of signal observations in a block, and (c) performance decrease with an increase in the number of transmit elements, which is to be expected given the accompanying increase in the bit rate.

Part I

Introduction

Chapter 1

The Underwater Acoustic Channel

Underwater acoustic channels (UWA) are considered to be one of the most difficult media for communication. Acoustic propagation is better on low frequencies while at high ones attenuation blocks high range transmissions. Due to the nature of the signal, the bandwidth of the systems is very limited and usual designs operate within a few tenths of kHz. As the center frequency is comparable to its bandwidth, the systems are considered to be wideband. For this reason, channel frequency response is not flat and strong fades are present because of the multipath. Low speed propagation of the sound, $1500m/s$ approximately, causes high end to end delays and a remarkable Doppler effect. Following sections explain more deeply each one of these characteristics.

1.1 Attenuation

One of the consequences of the systems to be wideband is that attenuation is depending on the frequency. This dependence is consequence of energy absorption of the mechanical waves and spreading loss increasing with distance. The expression for the attenuation can be expressed as

$$A(d, f) = (d/d_r)^k a(f)^{d-d_r} \tag{1.1}$$

Being d the transmission distance, d_r is taken as a reference, k is the propagation constant which values are usually between 1-2 and $a(f)$ is an increasing function of the frequency, see figure 1.1. The analytical expression for the absorption coefficient corresponding to the previous cited figure was found empirically

$$a(f)_{dB/km} = 0.003 + \frac{0.11f^2}{1+f^2} + \frac{44f^2}{4100+f^2} + 2.75 \cdot 10^{-4} f^2 \tag{1.2}$$

Where f is expressed in kHz.

1.2 Noise

For ambient noise in UWA channels there are many sources to consider such as waves, ships, turbulence and thermal noise; however, the latter is not so important for shallow water channels. Noise can be considered as Gaussian although it's not white. It is more important in low frequencies while in the high part of the spectrum it decays as $18dB/decade$ like show in figure 1.2. A good approximation is

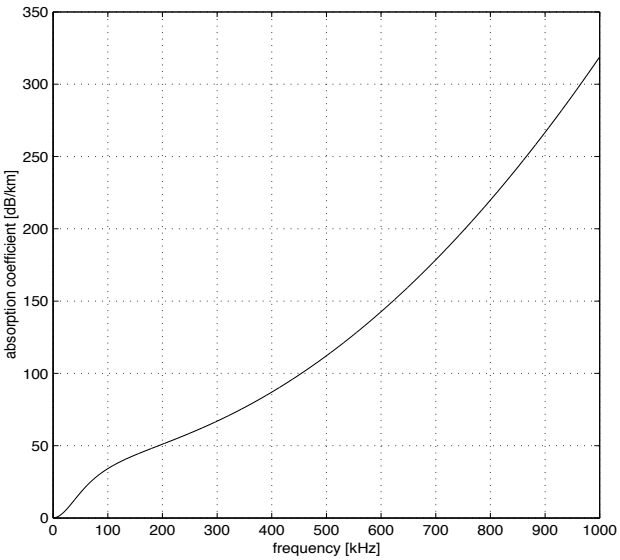

Figure 1.1: Absorption coefficient in [dB/km]

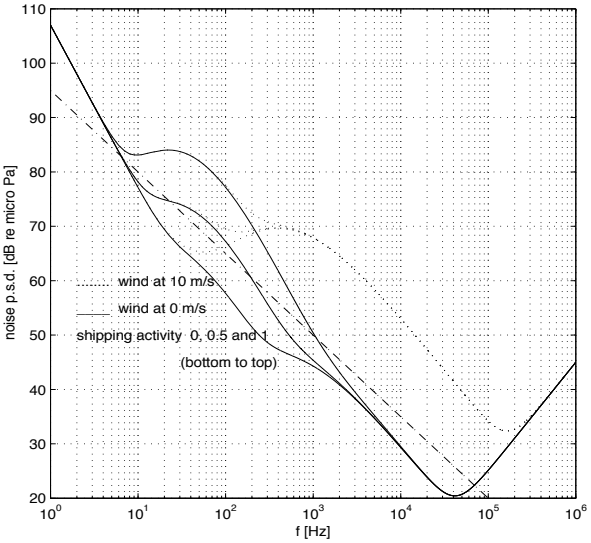

Figure 1.2: Sources of ambient noise and analytical approximation

$$N(f)_{dB} = \eta_0 - 18logf \tag{1.3}$$

And η_0 deppends on the situation and it is experimentally determined. Knowing attenuation and noise, an expression for the Signal to Noise Ratio is available (SNR) depending on the transmission distance and the frequency.

$$SNR(d,f) = \frac{S_d(f)/A(d,f)}{N(f)} = \frac{S_d(f)}{A(d,f)N(f)} \tag{1.4}$$

$S_d(f)$ is the transmitted power spectrum of the signal. Equation (1.4), if evaluated, shows that for each transmission distance there is an optimum frequency where the SNR ratio is a maximum. Vast literature is found on this topic see [3]. This fact is very important when designing networks and transmission systems, figure 1.3.

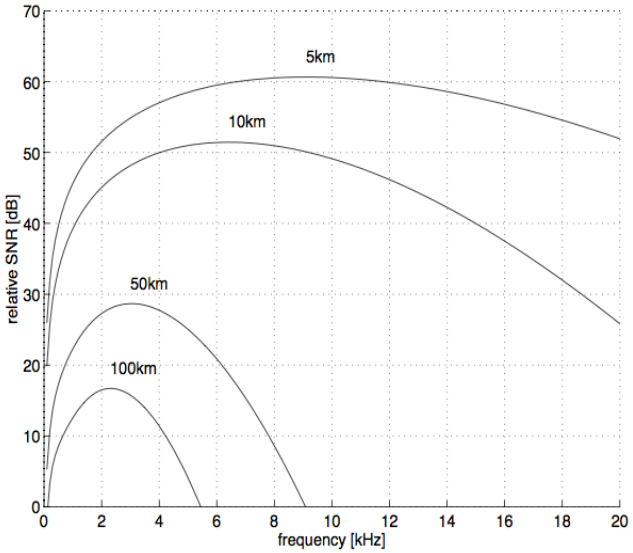

Figure 1.3: SNR depending on the frequency and transmission distance for a fixed transmitted power

1.3 Multipath

The effects of multipath in shallow waters are mainly reflections in the surface, in the bottom and in possible objects that are in the scene. These reflections are the responsible for causing multiple arrivals to the receiver. Channel impulse response (CIR) expression can be calculated knowing the channel geometry, the frequencies of operation and the sound speed profile, which can vary depending on weather conditions such as temperature and wave height. A general form of it is

$$h(t) = \sum_{p=0}^{P} h_p \delta(t - \tau_p) \tag{1.5}$$

Where h_p are the paths amplitudes and can be considered as a low pass filter due to channel attenuation properties. Multiple arrivals are the roots of fading since interference of different paths can be constructive or destructive. Simplified models for the fading are commonly accepted in UWA channels, like Rayleigh or Rician.

1.4 Doppler Effect

In this section differences between Doppler shift and Doppler spectrum will be made. The former is the frequency displacement while the latter is closely related to channel time coherence. A more detailed explanation follows.

Doppler shift This effect, caused by the relative motion of two bodies, is of special importance in underwater channels. The low speed of sound, which is about $c = 1500$ m/s and varying slightly with the speed profile , is the principal cause of this effect. Waves and currents make both the transmitter and receiver elements to be in continuous movement even if they are still on the bottom. The frequency shift, exactly as in mobile radio channels, is proportional to $\Delta f \propto \frac{v_r}{c}$ which means that if

c, the wave propagation speed, is low then the shift will be higher. In mobile radio channels shifts are of little interest in most of the cases, but in UWA channels this effect must be taken into account.
One assumption on radio channel is that the Doppler shift is uniform all over the bandwidth. This is true, as the frequency shift is proportional also to the carrier frequency, only if $BW << f_c$. In UWA channels this approximation cannot be fulfilled since the system bandwidth is comparable to its center carrier frequency. This leads then to non uniform Doppler shifts [4] and the signal spectrum expands or contracts depending on the relative motion. As a consequence, the duration and bandwidth of the signal are not the same and new values are $T_d = T/(1+a)$ and $B_d = B(1+a)$ being a the Doppler factor.

Doppler spectrum The models behind Rayleigh or Rician fading assume that many waves arrive each with its own random angle of arrival (thus with its own Doppler shift), which is uniformly distributed within $[0...2\pi]$, independently of other waves. This allows to compute a probability density function of the frequency of incoming waves. If we look at the Rayleigh fading channel in the time domain we find that the autocorrelation function of a specific tap (single arrival) is a first order Bessel function which depends of the maximum Doppler spread. We then can calculate the power spectral density (p.s.d.) of the Doppler, which shows how much the channel spreads the signal. For example, If a sinusoidal signal is transmitted, after transmission over a fading channel, we will receive a power spectrum according to a U-shaped function

$$D(f) = \frac{1}{2\pi f_d \sqrt{1-(\frac{f}{f_d})^2}} \quad |f| < f_d \tag{1.6}$$

Where f_d is the maximum doppler spread. In practice, signals have a much complex spectrum but the frequency range where the power spectrum is nonzero defines the Doppler spread. This somehow is related to the channel time coherence. More specifically, as said before, the inverse Fourier transform of the Doppler spectrum is the autocorrelation function of a channel tap in time. From there, channel time coherence t_c can be inferred. Usual approximations assume that $f_d \propto \frac{1}{t_c}$.

Doppler effect is of extreme importance when dealing with multicarrier communications. Little frequency variations can cause an important degradation in performance. Usually, frequency shifts are corrected with hardware via resampling due to the cost of the operation, while Doppler spectrum estimation can be done in a low-complexity manner once having the sampled signals.

Chapter 2

Orthogonal Frequency Division Multiplexing

2.1 OFDM Signals

OFDM is a frequency-division multiplexing (FDM) scheme utilized as a digital multi-carrier modulation method. A set of independent orthogonal subcarriers are used to transmit data. The total bandwidth is divided into a large number of narrowband channels each one non-interfering with each other.

System

A complete description of an OFDM system, which includes transmitter and receiver is shown in figure 2.1. An input serial data stream (we assume coding and interleaving are already performed) is converted first into K streams, where K is the number of subcarriers of the system. After mapping the bits into the symbol space with a proper modulation, namely a generic QAM, some subcarriers can be reserved to insert pilot symbols. Each band is then modulated with an specific frequency, see section 2.1 for a detailed explanation, and afterwards guard intervals and up-conversion are added and performed respectively. Finally, the signal is transmitted and sent through the channel. The dual process process is executed on the receiver side to retrieve the original bit sequence.

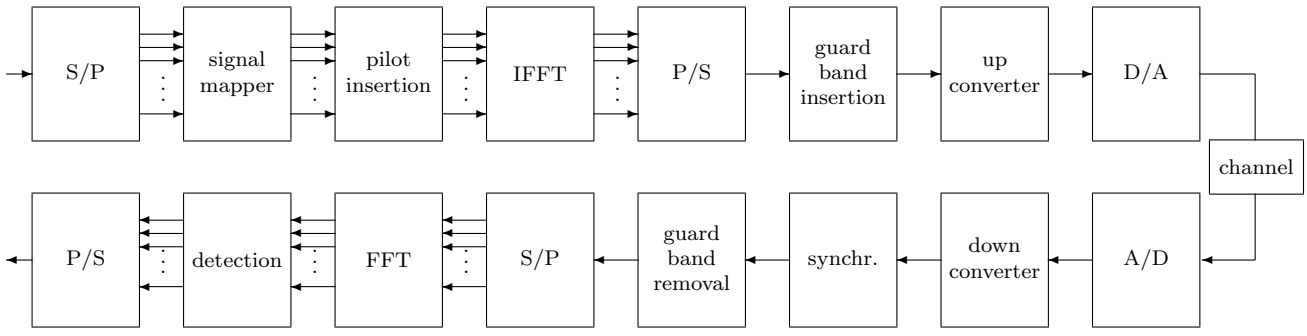

Figure 2.1: Typical block diagram of an OFDM system

Mathematical description

In this section a former description of the OFDM signals is shown. It is important to know that OFDM is formed by blocks each containing the transmission for the K subcarriers. Each block duration contains the effective symbol time and the guard interval

$$T = T' + T_g \tag{2.1}$$

Where T_g stands for the guard time and it must be longer than channel impulse response length to prevent inter-symbol interference between two consecutive OFDM blocks. T' stands for the effective symbol duration and it is defined as $T' = B/K$ where B is the overall system bandwidth and K is the number of subcarriers, the spacing between adjacent subcarriers is $\Delta f = 1/T'$. So, the subcarrier frequencies are:

$$f_k = f_0 + k\Delta f, \quad k = 0 \dots K-1, \tag{2.2}$$

where f_0 is the optional carrier frequency for a not baseband transmission. Each of the subcarriers contain a QAM symbol; typical modulations on the UWA channel are QPSK, 8PSK and low density QAM such as 16 or 32-QAM. It is assumed that all the subcarriers contain the same modulation level; unlike the Discrete Multitone Modulation (DMT) where each subcarrier varies the bandwidth efficiency depending on the SNR in that band.
From the OFDM definition we can derive an expression for the bandwidth efficiency, which is the ratio for the bit rate to the bandwidth

$$\frac{R}{B} = \frac{m\alpha}{1 + T_g B/K} \tag{2.3}$$

Where m stands for the modulation level and its units are $bits/symbol$ and for the case of QPSK is $m = 2$ $bits/symbol$. α is the coding efficiency, either for block or convolutional coding. In (2.3) it is clearly seen that the efficiency of the system increases as spacing between subcarriers B/K and the guard interval decrease.
Each one of the mapped symbols is modulated with one subcarrier, that is if the symbol on the k-subcarrier is called d_k then the baseband expression of the modulated signal for only one block is

$$b_s(t) = \sum_{k=0}^{K-1} d_k e^{j2\pi k\Delta f t} \quad t = 0 \dots T' \tag{2.4}$$

Equation (2.4) has the form of an IFFT operation. In fact, all the practical modulation schemes implement the OFDM modulation process as an IFFT due to its low-complexity and dedicated existing hardware. In the receiver side, an FFT will be key to retrieve the data. To transmit the signal, a guard interval must be added. This can be in the form of Cyclic Prefix (CP) or a simple Zero Padding (ZP) operation [5]. The first one is used in most of the radio systems for its capability to preserve the FFT/IFFT circularity converting a linear channel convolution into a circular without any additional processing and offering good synchronization via autocorrelation on the receiver. The latter is used when power saving is needed and it offers even better properties than CP, but additional computations should be done to the received signal. The expressions for each one of the

signals is given by

$$b_s(t) = \sum_{k=0}^{K-1} d_k e^{j2\pi k\Delta f t} g_{ZP}(t) \quad t = 0 \dots T \quad \text{for ZP} \tag{2.5}$$

$$b_s(t) = \sum_{k=0}^{K-1} d_k e^{j2\pi k\Delta f (t-T_g)} \quad t = 0 \dots T \quad \text{for CP} \tag{2.6}$$

The $g_{ZP}(t)$ function is a rectangular pulse with duration T and it represents the zero-padding operation. Once known the baseband expression of the signal, the sent signal is

$$s(t) = \Re\left\{ \; b_s(t) e^{2\pi f_0 t} \; \right\} \tag{2.7}$$

Therefore, $s(t)$ represents an OFDM symbol containing K symbols. The spectrum of a typical OFDM signal is like the one shown in figure 2.3 The effective block symbol time is

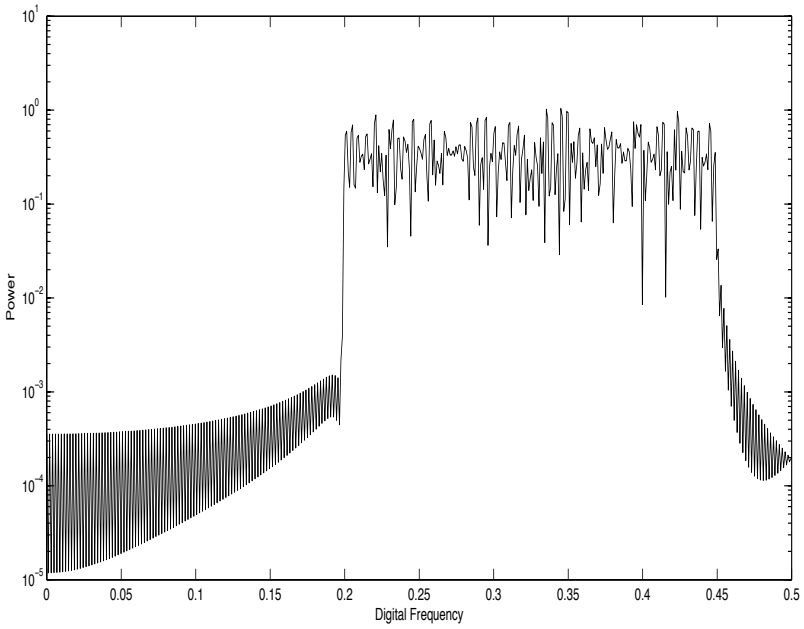

Figure 2.2: OFDM Signal Spectrum with $K = 128$ subcarriers

related to the subcarrier spacing to preserve the orthogonality between subcarriers. That is, for two specific subcarriers $\phi_k(t), \phi_l(t)$ in the demodulator

$$\int_0^{T'} \phi_k(t)\phi_l(t)^* = \int_0^{T'} e^{j2\pi k\Delta f t} e^{-j2\pi l\Delta f t} = \delta(k-l) \tag{2.8}$$

Where $\delta(t)$ is the Kronecker's delta. The orthogonality can be thought in time or in frequency domain. In time domain, as stated in previous equation, each subcarrier is a sine wave with an integer number of cycles within a block so, the definition of a scalar product of two sine waves with multiple frequencies is zero. From the frequency domain, the spectrum of each subcarrier is a *sinc* function with its maximum value in its center frequency while being zero at other subcarriers' centers.
Although the modulation process is very simple, there are some practical mathematical

advices to be aware of. Let's assume that the sampling frequency is f_s and the number of samples of an OFDM block is N_s. When generating the signal in the frequency domain, an IFFT of at least $2K$ samples has to be done in order to verify the Nyquist theorem to prevent aliasing. Then a condition that must be satisfied always is $N_s > 2K$. Moreover, if the signal is translated to an upper band before D/A conversion, this condition has to be more strict and becomes $f_s = N_s/T' > 2(f_0 + \Delta f K) = 2B$.
In the receiver side, accurate synchronization is needed. Whichever type of chosen OFDM, CP or ZP, the guard interval has to be removed prior to FFT demodulation. Synchronization and guard removal are processes that differ depending on the chosen scheme, [5] exposes them in a more detailed manner.

Coding and Interleaving

In order to keep the bit error rate probability low, or even an error free communication; coding and interleaving are needed to reduce incorrect detections. Usually, when using an OFDM modulation, the system is considered wideband. Therefore, as the frequency response of the channel is not equal for each subband, there can be parts of the spectrum which are more error prone due to their high attenuation and low SNR ratio. In this section, an overview of some possibilities are outlined.

Coding Like in all other communications systems, in the useful bits that have to be sent some redundancy is added. Channel coding, differenced to source or entropy encoding, is used to protect data sent over the channel even in the presence of noise. the redundancy added makes possible to retrieve the error-free original bits if the coding is properly dimensioned. That is, depending on the SNR ratio, more redundancy has to be applied. Shannon established a theoretical limit for the rate of the communications.

$$C = BW \times log_2(1 + SNR) \quad bps \tag{2.9}$$

The channel capacity, C, is directly proportional to the bandwidth used. When designing a system the coding used has to respect this limit, if any knowledge of prior SNR is available. Otherwise errors will appear on the receiver side.
Two types of coding are mostly used in actual systems: block and convolutional coding. The main difference between them is that the former transforms blocks of useful bits into codewords properly designed while the output of the latter is formed based on bit operations. To decode a block coding the received bits are assigned the closest codeword and then retrieve the original bits. To decode a convolutional coding, the Viterbi algorithm is needed.

Interleaving This technique by itself, doesn't help to reduce the number of errors but to make them look random. In communications, errors usually appear in bursts. These errors overwrite several bits in a row, so a typical error correction scheme that expects errors to be more uniformly distributed can be overwhelmed. Formally speaking, the main purpose of interleaving is to change the probability distribution function of the errors and make them appear independent from others.
In OFDM two types of interleaving are possible: frequency and time interleaving. The first one is possible as the data is transmitted in parallel and independent subcarriers, while the second is possible because each sent block is independent of the others. The main drawback of the time interleaving is that a delay on the detection

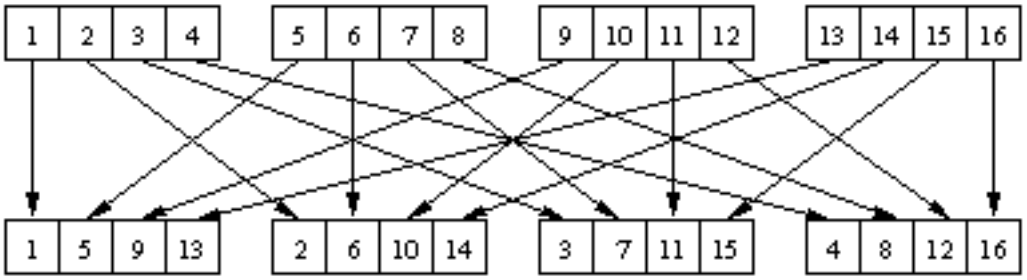

Figure 2.3: Example of time interleaving with the original and the interleaved data (top and bottom respectively).

is introduced but as an advantage it protects the data from burst errors. Frequency interleaving is useful to deal with the non-flat channel frequency response so, error within an OFDM also are more uniformly distributed with no delay expenses.

Advantages, Drawbacks and System Design

In this section the main advantages and drawbacks of an OFDM system.
Advantages

- Can easily adapt to severe channel conditions without complex equalization
- Robust against narrow-band co-channel interference
- Robust against Intersymbol interference (ISI) and fading caused by multipath propagation
- High spectral efficiency
- Efficient implementation using FFT
- Low sensitivity to time synchronization errors

Drawbacks

- Sensitive to Doppler shift.
- Sensitive to frequency synchronization problems.
- High peak-to-average-power ratio (PAPR), requiring linear transmitter circuitry, which suffers from poor power efficiency.
- Loss of efficiency caused by Cyclic prefix/Guard interval.

Although there are some important factors in the drawbacks' list, OFDM is the best candidate to support high rate underwater communications.

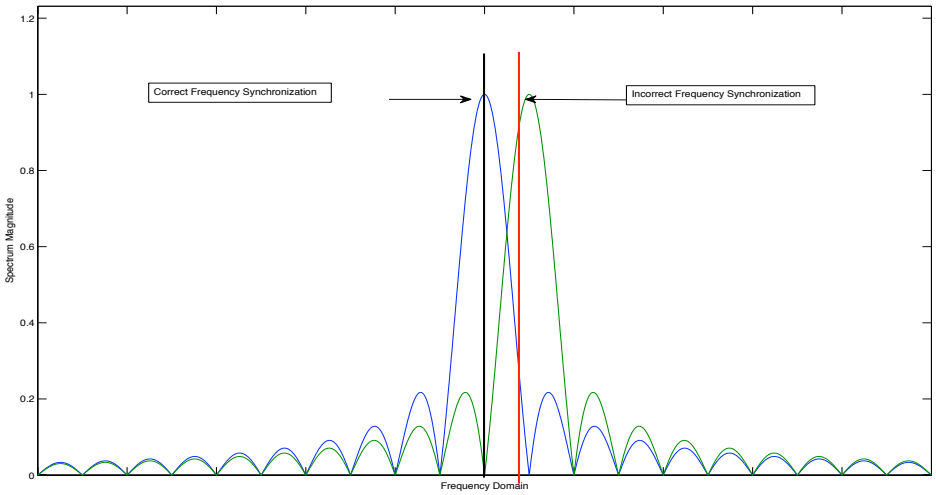

Figure 2.4: Frequency synchronization in OFDM systems.

2.2 Intercarrier Interference

One of the main causes of performance degradation is Intercarrier Interference (ICI). The main advantage of OFDM is that each subcarrier is orthogonal, and thus independent, to each other. When the channel conditions change, this orthogonality disappears and then, each subcarrier has some contribution to the others in the demodulating process. In this section, the sources of ICI are presented and a new OFDM signal model is also shown.

Sources

Although there can be many processed that can cause ICI here we will focus on the ones that are more important in underwater communications.

Doppler Shift As shown in section 1.4, the UWA channel suffers from severe Doppler effect due to the low carrier frequencies and the low speed of propagation of sound. The main cause of this effect is the relative motion between the ends of the transmission. As a further matter, the wideband nature of the signal impacts in two ways in its transformation. A frequency shift, and a time (de)compression. Recall from radio channels that time consequences are neglected in most of the cases and only frequency shift is considered. When talking about wireless OFDM in UWA communications it should be known that the Doppler shift can be sometimes comparable or even more than the subcarrier spacing. Conventionally, this shift is combated via resampling in time domain of the data, but its offset has to be known precisely. Produced ICI due to frequency de-synchronization is shown in figure 2.4. It can be seen that if correct synchronization is performed, no influence of any subcarrier is collected (although the example only shows two subcarriers for clarity, this can be extend to an arbitrary number). If the receiver oscillator has a little offset, or if there has been some uncorrected Doppler shift, incorrect synchronization is then

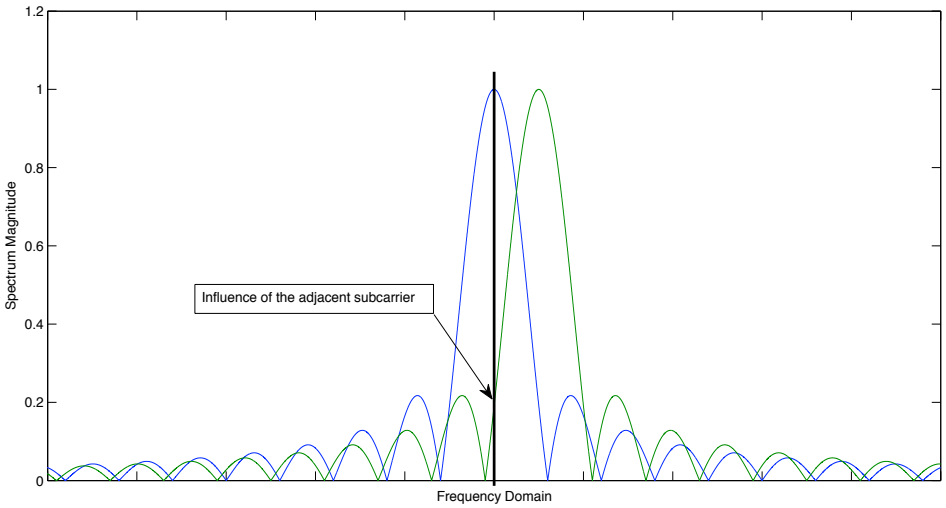

Figure 2.5: Effect of the Doppler spread in the ICI phenomenon

performed in the receiver and influence from other subcarriers are collected for one band as shown with the red line in the figure.

Channel Time-Variance and Doppler Spread In OFDM, the channel is supposed to be time invariant within a block. If this condition is not satisfied, again, the subcarriers loose their orthogonality. Mathematical expressions are available if some assumptions about the Doppler spread are maid [6]. Intuitively, figure 2.5 shows how this effect can lead to a degradation of the performance.
Coherence time of the UWA channel is a critic paramter. Unlike radio communications, the lack of high bandwidths can make a transmission of an OFDM block with a high number of subcarriers last for a few milliseconds. In this time, the channel can change noticeably and time invariability is no longer respected. In practical situations, observations of the channel show that its coherence time can be of about $t_c = 200$ ms or less. As the Doppler spread f_D is inversely proportional related to t_c, section 1.4, a spread of a few Hz is present in the system. There are some real systems deployments which consider a subcarrier spacing of about 10Hz (a 1024-OFDM with 10KHz bandwidth, for example). Those system will suffer of severe ICI, if nothing is done about it.

Signal model

If ICI has to be considered, a more complex mathematical model arises. Although analytical expressions can be derived making reasonable assumptions on the channel. Most of the systems don't need to be very accurate and simply model the received signal for one block as:

$$y_k = \sum_{m=0}^{K-1} H_{m,k} d_m + w_k \tag{2.10}$$

This simple model clearly shows that each received subband y_k has the influence of all the other subcarriers. $H_{m,k}$ stands for the coefficient of the channel that represents the

influence of the subcarrier m to the subcarrier k and usually, in almost ICI-free systems, $H_{k,k} >> H_{m,k}$ when $m \neq k$. A closed expression can also be found for the coefficients $H_{m,k}$ in terms of the time variant CIR $h_n(l)$

$$H_{m,k} = \frac{1}{K} \sum_{n=0}^{K-1} \sum_{l=0}^{L} h_n(l) exp\left(j2\pi \frac{n(m-k) - ml}{K} \right) \tag{2.11}$$

If the channel impulse response $h_n(l)$ does not depend on the index n, only the coefficients $H_{k,k}$ are non-zero and system is ICI free. This is however not real in practical systems. If we desire to simplify even more the model, we will simply separate the non-ICI part from the interfering one and lead to

$$y_k = H_{k,k} d_k + ICI_k + w_k \tag{2.12}$$

The main drawback with this equation is that ICI is treated as additional noise. If its power is negligible, this approximation can result in good performance without increasing system complexity, but if the power of the other subcarriers is somewhat important, then a more complex model, and yet a more complex system has to be taken into account, [6].

Chapter 3

MIMO Systems overview

MIMO, Multiple-Input Multiple-Output, is an antenna technology where multiple antennas are used in both ends of a transmission. Therefore, either in transmitter and/or receiver more than one antenna is deployed. This technique allows to increase the bit rate of the communications link without need to increase the transmitter power per antenna nor the bandwidth. These systems are defined by its spatial diversity and multiplexing, namely the number antennas used in both sides of the system.
Spatial Multiplexing is defined as the transmission of multiple data streams over more than one antenna. Two types have to be taken into consideration, V-BLAST (firstly used in Bell Laboratories) and Space-Time Codes, which use orthogonal data streams for a better detection on the receiver. See references for a more detailed information
Spatial Diversity is the source of improving channel capacity (multiplexing decreases it). The diversity is based on structured redundancy as the signal sent from one antenna is received in all the others. If the MIMO channel suffices some conditions, the system can retrieve the original sent signals from the received ones.

3.1 Forms of MIMO

Like many systems, MIMO exist in different forms as in figure 3.1. In the latest standards, such as the IEEE 802.11n or WiMAX, spatial diversity is used offering very good results in terms of capacity and bit rate. There are, though, many drawbacks of the technique and the number of transmitters is often limited to 4 in most of the standards. There are two main reasons, the first one is because each of the antennas has to be away of the other in order to make the received signal uncorrelated with the others, hence, more deployed antennas mean a bigger transmitter and/or receiver. The second one is because of over-multiplexing and the MIMO channel, see section 3.2.

Single-Input Single-Output

This case cannot be considered an innovation scheme. The system is a conventional communications system with one transmitter and one receiver. Nevertheless it is not of less importance because nowadays there are still many systems that use this architecture. MIMO, for a proper behavior, needs multipath propagation to create a certain number of uncorrelated and independent channels. In many situations, both transmitter and receiver have a line of sight and little spatial diversity can be created.

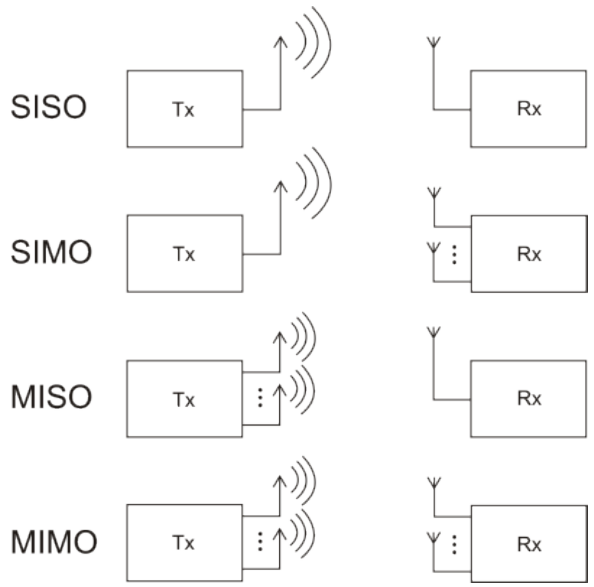

Figure 3.1: Different forms of MIMO and their configuration

Single-Input Multiple-Output

In this situation, multiple receivers are deployed, all receiving the stream sent from one transmitter. In this situation, Maximal Ratio Combining (MRC) can be done at the receiver side, thus combating with strong multipath fades. The combination of the received signals is performed maximizing the resultant SNR and it's optimal for AWGN channels.

Multiple-Input Single Output

For this degenerated form, special coding is needed in the transmitters. The transmitters have to send otrhogonal streams to make the detection possible in the receiver. Section 3.3 exposes some principles about space-time coding but although this coding can be used in other system configurations, it is not usual to have a system where the number of transmitter is higher than the number of receivers.

Multiple-Input Multiple-Output

This is the general form of the spatial diversity systems and although the advantages of MISO and SIMO configurations are present, the system complexity also increases. Nowadays, advanced forms of MIMO are being developed, mainly using multiuser, but this document will only refer to the classical approach.

3.2 The MIMO channel

To understand the principles of MIMO, a mathematical approach is needed. As seen in figure 3.2, each of the transmitter antennas contribute to the received signal in each one of the receivers For a channel model, we will consider a narrow band, flat fading channel and the expressions will be used in the frequency domain. For instance we can express

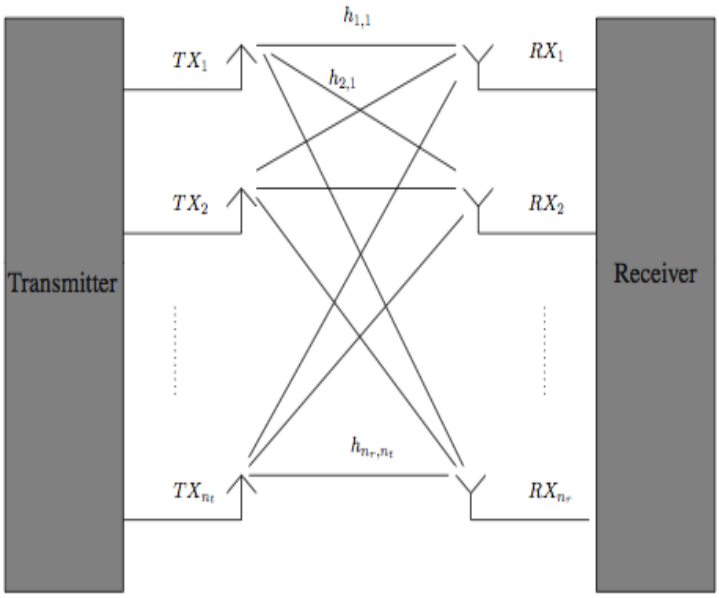

Figure 3.2: Simplyfied scheme of the MIMO channel

the received signal for one antennas as

$$y_{f_0}^r = \sum_{t=1}^{M_t} H_{f_0}^{tr} d^t + w_k^r \quad r = [1 \dots M_r] \tag{3.1}$$

Where t, r stand for the transmitter, receiver index and f_0 is the frequency of operation. Time index is dropped because of notation simplicity. M_t and M_r refer to the number of transmitters and receivers of the system respectively. For clarity, we will express the previous equation in matrix notation. Defining the vectors

$$\mathbf{y_{f_0}} = [y_{f_0}^1, \dots, y_{f_0}^{M_r}] \tag{3.2}$$

$$\mathbf{d} = [d^1, \dots, d^{M_t}] \tag{3.3}$$

$$\mathbf{w_{f_0}} = [w_{f_0}^1, \dots, w_{f_0}^{M_r}] \tag{3.4}$$

$$\tilde{\mathbf{H}}_{f_0} = \begin{bmatrix} H_{f_0}^{1,1} & \dots & H_{f_0}^{M_t,1} \\ \vdots & \ddots & \vdots \\ H_{f_0}^{1,M_r} & \dots & H_{f_0}^{M_t,M_r} \end{bmatrix} \tag{3.5}$$

The expression in equation (3.1) becomes then

$$\mathbf{y}_{f_0} = \tilde{\mathbf{H}}_{f_0} \mathbf{d} + \mathbf{w}_{f_0} \tag{3.6}$$

Once we can express the received signal in a more compact form, analysis of the equation can be done. It is clear from equation (3.6) that each transmitter contributes to all the receivers and that some conditions on the channel matrix $\tilde{\mathbf{H}}_{f_0}$ will be necessary to demodulate the original signal $\mathbf{d}$.
Other than going further with the demodulation process we will take a closer look at the physical representation of this equation. As Shannon already did for simple SISO systems, the channel capacity can also be computed for MIMO configurations. The principles are

the same, the capacity will be the maximum mutual information between the data before the channel, $\mathbf{d}$ and the data received, $\mathbf{y}$. The usual expression for a flat fading channel is:

$$C^{M_t,M_r} = max\{I(\mathbf{d},\mathbf{y})\} = \max\, E_{\tilde{\mathbf{H}}_{f_0}}\{log_2 det\left(\mathbf{I}_{M_t} + \tilde{\mathbf{H}}_{f_0}\mathbf{R}_d\tilde{\mathbf{H}}'_{f_0}\right)\} \tag{3.7}$$

Some considerations about the previous equation:

- If the channel is deterministic, the expected value is not used. If the channel random, averages are needed and then the term *ergodic capacity* is used
- The matrix R_{d_k} represents the correlation of the sent bits. This matrix is mainly the power allocation on the transmitters.
- Channel capacity is only useful in the transmitter side. Consequently, channel state information (CSI) is needed at the transmission side of the communications system.
- If no CSI is available, no techniques on power allocation can be done, hence, the same amount of power will be transmitted in each of the antennas.
- The strategy ot maximize the capacity depends on the type of fading assumed for the channel. Rayleigh, Rician and Nakagami channels are the models used in typical situations.

Numerous studies have been done for the MIMO channel. This document will not focus on the statistical characterization of the UWA MIMO channel but more on demodulation techniques that can be applied.

3.3 Space Time Coding

The Space Time Coding is a techniques used to improve reliability in a MIMO link. Redundancy is introduced in the transmitters with the hope that forward error correction (FEC) on the receiver will recover the original, useful data. Space time codes may be divided into two subgroups:

Space Time Trellis Codes STTC Much complex than block codes, this types of codes distribute a trellis code into several antennas thus providing diversity and coding gain. As the trellis coding is convolutional the receivers relies on the Viterbi algorithm to decode the data, thus increasing the system complexity.

Space Time Block Codes STBC This technique is based on constructing a set of orthogonal codewords which are transmitted along the antennas. the complexity of it is much less that STTCs and only linear operations are needed.

Since STTCs are far more complex, STBCs will be explained in a more detailed manner. In the system deployed in SPACE'08 experiment Alamouti Coding was used.
In each time block, a total of M_t symbols are received. These symbols can be expressed in a matrix forming a space-time symbol which will define the coding type:

$$\mathbf{D} = \begin{bmatrix} d_0^1 & \dots & d_{N-1}^1 \\ \vdots & \ddots & \vdots \\ d_0^{M_t} & \dots & d_{N-1}^{M_t} \end{bmatrix} \tag{3.8}$$

Where d_j^i represents the symbol sent on the transmitter i at time instant j. The main point of the coding is to make the set of codewords, that is $d_j^i, \forall i$ orthogonal between each other. The result of this is simple, linear and optimal decoding at the receiver. As many coding techniques, the use of redundancy make the system sacrifice its data rate. The rate of the code is given by the number of encoded symbols in one time block (note that many transmitters can send the same symbol) divided by the number of time slots necessary to complete the sapce-block symbol, $r = \#symbols/N$. The simplest of these codes is the Alamouti's code, with a matrix of 2×2 with no bit rate loss as its rate is 1. The matrix for this code is

$$\mathbf{D} = \begin{bmatrix} d_1 & d_2 \\ -d_2^* & d_1^* \end{bmatrix} \tag{3.9}$$

Where it can be seen that the columns od the matrix are clearly orthogonal. In the receiver side, using optimal decoding scheme, the bit-error rate (BER) behavior of the Alamouti's code is equivalent to a MRC of 2 symbols over M_r receivers. This is a result of the perfect orthogonality between the symbols after receive processing: there are two copies of each symbol transmitted and M_r copies received. Maximum likelihood decoding is performed with the only need of linear operations, thus maintaining the system complexity low. Recall that the symbols will not be recovered after 2 time slots (N for a general STBC) thus introducing a little delay.
Although the commented scheme was for STBCs, STTCs are more robust against errors, but the receiver complexity is higher as dynamic programming algorithms are needed on the receivers for correct data decoding. Either way, the use of space time coding permits to MIMO systems to operate with more transmitters than receivers.

3.4 MIMO OFDM

When the MIMO channel was presented in previous sections, a flat fading model was assumed. This is not true for a wideband system, where the channel has really different responses for each part of the spectrum. For instance, strong fades due to multipath can cause variations over 20 dB and the model for the MIMO capacity is no longer respected. One of the reasons why OFDM is a good associate for a MIMO transmission is because it divides the overall spectrum into a set of narrow band, flat fading channels. This indeed creates a group of independent channels, and each one of them accomplish the MIMO conditions presented before.
The capacity is then the sum of each one of the narrow-band capacities. Obviously, if some subband has less attenuation that others and a better SNR, a higher level modulation can be employed in this band. Many wireless systems take profit of the subband independence, such as xDSL technologies, and transmit a different number of bits for each subband. For this to be possible CSI at the transmitter must be present. However in UWA channels no feedback information from the receiver can be sent to the transmitter faster than the time coherence of the channel, hence, uniform power allocation (UPA) and the same type of modulation is used for all the subbands in OFDM.

Part II

Data detection Algorithms

Chapter 4

State of the Art of OFDM UWA Systems

All along this chapter some of the existent algorithms for OFDM demodulation will be outlined. Plenty of work has been done in this area since OFDM is a promising technique for high rate communications with wideband signals. UWA channels per se, are one of the most difficult channels for data transmission. Previous transmission techniques were tried for underwater communications such as spread spectrum or single carrier modulations for example. With the arrival of OFDM, the receiver and transmitter complexity decreases achieving high efficiencies. Due to OFDM scalability the data rate can be varied significantly so, each communication link can be tuned easily to have the maximum possible bit rate.
The purpoes of this document is to apply one algorithm for a MIMO system with data of the SPACE'08 experiment and see the results. Additionally, some ideas about ICI are considered.

Low-complexity OFDM detector

This algorithm, in contraposition with the previous one, makes all the processing post FFT. The technique in [4] dealt with the resampling frequency and modified the signal before the FFT operation. Although the Doppler shifts that can be corrected via hardware are higher than the ones only using software, its simplicity makes it worth mentioning. The algorithm in [1] makes uses of multiple receiver MMSE combining and separes phase tracking from equalization using a Doppler model for the phase change, see figure 4.1. Let's define the received signal vector for a given subband

$$\mathbf{y}_k(n) = \left[y_k^0(n) \dots y_k^{M_r}(n)\right] \tag{4.1}$$

Where the expression of each received signal $y_k^r(n)$ for receiver r and OFDM block index n can be seen as

$$y_k^r(n) = H_k^r(n) d_k e^{j\theta_k(n)} + z_k(n) \tag{4.2}$$

Where H_k is the frequency response of the channel at the subband k for $0 \geq k < K$. The term $\theta_k(n)$ is the time-varying phase offset. The matrix notation for all the receivers is

$$\mathbf{y}_k(n) = \mathbf{H}_k(n) d_k e^{j\theta_k(n)} + \mathbf{z}_k(n) \tag{4.3}$$

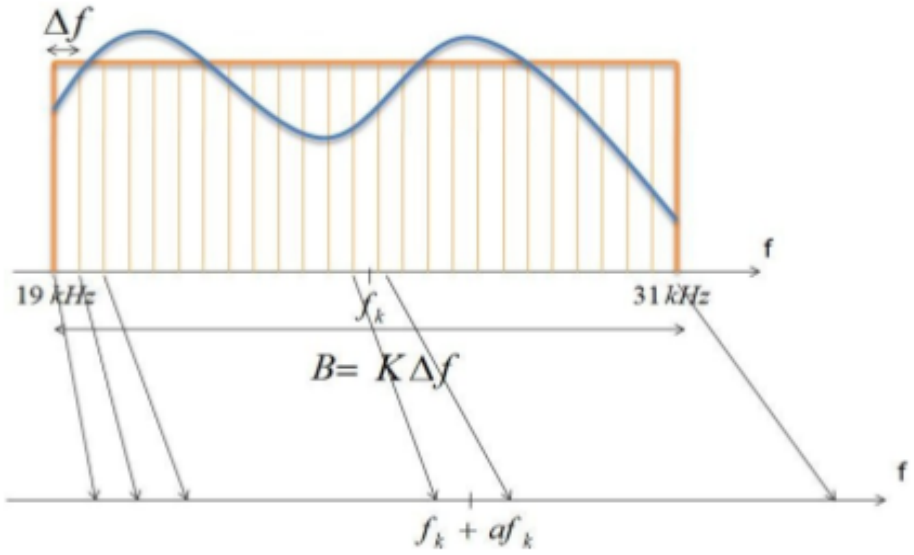

Figure 4.1: Example of non-uniform Doppler shift

Supposing that a channel and phase estimation are available for time n then an MMSE solution for the symbols is possible

$$\hat{d}_k(n) = \left[\sigma_z^2 + \mathbf{H}'_k(n)\mathbf{H}_k(n)\right]^{-1} \mathbf{H}'_k(n)\mathbf{y}_k(n)e^{-j\theta_k(n)} \tag{4.4}$$

From here, the assumptions on the algorithm on the channel to vary slowly from one OFDM to another, while the phase has to be updated. The model of the phase is of the form

$$\theta_k(n) = \theta_k(n-1) + a(n)2\pi f_k T' \tag{4.5}$$

Usually, the real values of the channel and the phases are not available but an estimate of them is used. For instance, the estimation of the channel of the previous block is used when demodulating the symbols from the current OFDM block, but the phase has to be updated. In figure 4.2 a graphic diagram of the algorithm is shown. The output of the

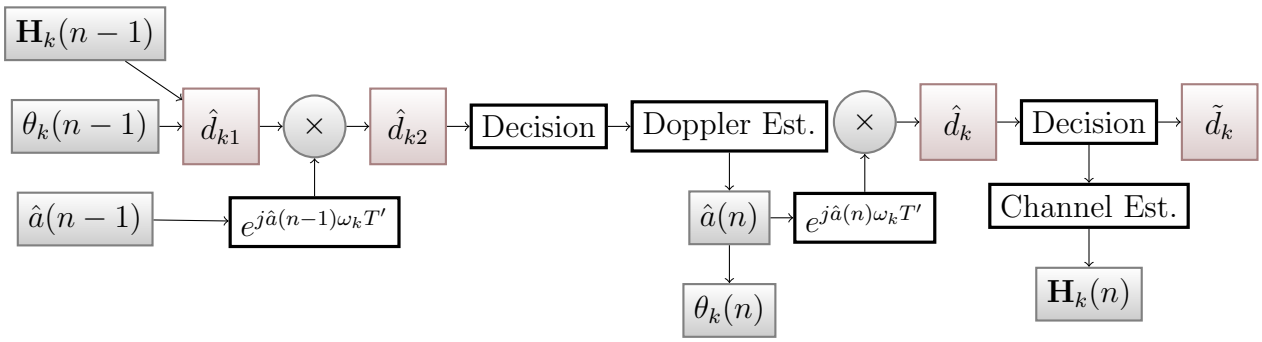

Figure 4.2: Diagram of the algorithm described in [1]

algorithm is the symbols $\tilde{d}_k$. The main points of the algorithm are the channel and the Doppler factor estimation. And in this document we present a more detailed version of these parts:

Phase tracking

In UWA channels, the main form of phase distorsion is the Doppler effect. Even if both ends of the transmission are still on the bottom of the sea, waves and currents make the paths arrive with some Doppler shift. In the algorithm [1] it is assumed that all the paths have the same scaling Doppler factor, characterized by $a(n)$, but different between OFDM blocks. An adaptive algorithm can be modeled for the phase variation. Namely, if we consider that each frequency f_k has a shift proportional to it like

$$f'_k = (1 + a(n))f_k \tag{4.6}$$

Knowing the relationship between phase and frequency (the first is the integral of the other in time domain), the phase variation is like the the one in equation (4.5). In the algorithm, the first symbol estimation, d_{k1}, calculated before phase updating can contain too large phase offset and a correction should be applied. Since it is assumed that the doppler factor varies slowly from one block to another, an update for its phase can be done easily using the Doppler factor estimate of the previous block leading to the first tentative symbol decision.
Once the first decided symbols, $\bar{d}_k$, are available, a more accurate Doppler factor is computed averaging the angular offset of d_{k1} with them as stated in (4.8):

$$\Delta\hat{\theta}_k(n) = \langle \hat{d}_{k1}(n)\bar{d}^*_k(n) \rangle \tag{4.7}$$

$$\hat{a}(n) = \frac{1}{K}\sum_{k=0}^{K} \frac{\Delta\hat{\theta}_k(n)}{2\pi f_k T'} \tag{4.8}$$

Only then, the new updated phases and the new symbols can be computed, leading to the final symbol decisions $\tilde{d}_k(n)$.

Channel Estimation

In all OFDM systems, channel estimation is one of the main parts of the algorithm, in this algorithm several approaches are possible. Although the use of pilots is common in many communications systems, the bit rate is decreased proportionally with the number of known symbols transmitted.
Usually, for channel estimation at least some of the symbols have to be known. Using a phase estimate $\hat{\theta}_k(n)$ and decided data symbols (which can contain pilots) it is possible to compute an unbiased estimate of the channel with the form

$$\hat{\mathbf{H}}_k(n) = \mathbf{y}_k e^{-j\hat{\theta}_k(n)} \tilde{d}^*_k(n) \tag{4.9}$$

It is possible, though, to use filtering with a forgetting factor λ to filter out high frequency components usually related with the noise. Although this channel estimation is performed on the frequency domain, thus needing K coefficients, a time domain estimation is also possible, reducing the computational cost.
The channel in UWA environments can extend to several milliseconds, but it has a sparse nature. Let's call the overall channel impulse response span in time L and the total arrivals J; usually, in a sparse channel, $J << L$. From the channel estimation on equation (4.9) we can find the CIR in the time domain defining the Fourier relationship:

$$\mathbf{H}_k(n) = \sum_{l=-A}^{L-1-A} \mathbf{h}_l(n) e^{-j2\pi kl/K} \tag{4.10}$$

Note that an UWA channel is rarely of minimum phase thus having arrivals before the strongest path. This means that the direct path between transmitter and receiver is not the fastest one, unlike the radio channel if a line of sight is available. After performing the IFFT, coefficients below a certain threshold γ can be eliminated as the channel will contain also noise and eliminating low energy taps can also reduce the noise variance. Thus, the channel CIR will be

$$\mathbf{h}_l(n) = \begin{cases} \mathbf{h}_l(n) & \text{if } |\mathbf{h}_l(n)| > \gamma \\ 0 & \text{if } |\mathbf{h}_l(n)| \leq \gamma \end{cases} \tag{4.11}$$

Different results are obtained for different γ, see section 7 for more details. Normally, γ is defined as $\gamma = \rho \times max(|\mathbf{h}_l(n)|)$ where ρ is between 0 and 1
The MIMO algorithm explained later in section 5 will use many of the equations shown in this section. In a simplified manner, the adaptation of this algorithm to multiple transmitters implies tracking of several Doppler factors, one for each transmitter, and a more difficult channel estimation because each pair of transmitter and receiver hydrophones has his own channel.

Chapter 5

Adaptive Algorithm for MIMO systems

The receiver algorithm used for data detection in the SPACE'08 experiment is the one explained in [2] and an overview is presented here commenting also the particularities of the MIMO channel. As a result of sending the signal through a channel, the received signal can be expressed in the frequency domain after the FFT demodulation as

$$y_k^r(n) = \sum_{t=0}^{M_t} H_k^{tr}(n) d_k^t(n) e^{j\theta_k^t(n)} + n_k^t(n) \tag{5.1}$$

Where t, r, k, n refer to the transmitter, the receiver the frequency index and the time respectively. H is referring to the channel frequency response and n to the noise component of the received signal. Using the expression (5.1) it is possible to construct an LS estimate of the received symbols in a matrix form:

$$\widehat{\mathbf{d}}_{k1}(n) = \mathbf{y}_k(n)\mathbf{H}'_k(n) \left[\mathbf{H}_k(n)\mathbf{H}'_k(n)\right]^{-1} \mathbf{\Theta}^*_k(n) \tag{5.2}$$

The prime denotes hemitian transpose and the asterisk complex conjugate. In practice, when the channels and the phases are not known, their estimates will be used instead of true values in the expression 5.2. Symbol decisions can then be made, e.g. by soft-decision decoding. Matrices and the vectors appearing in (5.2) are defined as

$$\mathbf{y}_k(n) = [y_k^1(n) \dots y_k^{M_r}(n)] \tag{5.3}$$

$$\mathbf{d}_{k1}(n) = [d_k^1(n) \dots d_k^{M_t}(n)] \tag{5.4}$$

$$\mathbf{H}_k(n) = [H_k^{tr}(n)]_{t=1\cdots M_t; r=1\cdots M_r} \tag{5.5}$$

$$\mathbf{\Theta}_k(n) = diag[e^{j\theta_k^t(n)}]_{t=1\cdots M_t} \tag{5.6}$$

The existing channel estimate $\widehat{\mathbf{H}}_k(n-1)$ is used to form two types of symbol estimates according to the expression (5.2): $\check{\mathbf{d}}_k(n)$ is obtained using the predicted phase $\check{\theta}_k^t(n)$ and $\acute{\mathbf{d}}_k(n)$ is obtained using the outdated phase $\widehat{\theta}_k^t(n)$. The former is used to make tentative symbol decisions $\overline{\mathbf{d}}_k(n)$, as the latter may contain too large phase offset. The underlying phase error is measured as

$$\psi_k^t(n) = \langle \acute{d}_k^t(n) \overline{d}_k^{t*}(n) \rangle, \forall k, t \tag{5.7}$$

And used to update the Doppler factors by averaging

$$\widehat{a}^t(n) = \frac{1}{K} \sum_{k=0}^{K-1} \frac{\psi_k^t(n)}{2\pi f_k T'} \tag{5.8}$$

These values are now used to update the phases according to (4.5). If the doppler distortion can be modeled as equal for all transmitters, which is not always possible, the expression (5.8) will include additional averaging over the transmit elements.

Channel estimation

The problem with (5.2) is that $\mathbf{H}_k$ has to be know. So, the problem is to estimate these coefficients having only the received signals as information. Let us define the Fourier relationship:

$$\mathbf{H}_k(n) = \sum_{l=-A}^{L-1-A} \mathbf{h}_l(n) e^{-j2\pi kl/K} \tag{5.9}$$

Where $\mathbf{h}_l(n) = [h_l^{tr}(n)]_{t=1,\cdots,M_t,;r=1,\cdots,M_r}$ represent the MIMO channel in the impulse response domain. Note that fewer than K impulse response coefcients may sufce to represent all of the K transfer function coefcients. In particular, we dene J as the number of signicant impulse response coefcients, and L as their total contiguous span. The Fourier relationship in (5.9) takes into account that the UWA channel is rarely of minimum phase so being $A \geq 0$, the impulse response will have an anticausal part. It is understood that $\mathbf{h}_l(n) = \mathbf{h}_{K+l}(n)$ for negative values of l. Putting together (5.1) and (5.9) and forming the matrices:

$$\mathbf{Y}(n) = \begin{bmatrix} \mathbf{y}_0(n) \\ \vdots \\ \mathbf{y}_{K-1}(n) \end{bmatrix} \quad \mathbf{D}_\theta(n) = \begin{bmatrix} \mathbf{d}_0(n)\mathbf{\Theta}_0(n) \\ \vdots \\ \mathbf{d}_{K-1}(n)\mathbf{\Theta}_{K-1}(n) \end{bmatrix}$$

We can express the received signal in a simple form:

$$\mathbf{Y}(n) = \sum_{l=-A}^{L-1-A} \mathbf{\Phi}^l \mathbf{D}_\theta(n)\mathbf{h}_l(n) + \mathbf{Z}(n) \tag{5.10}$$

Where $\mathbf{Z}(n)$ contains noise and defining the matrix as

$$\mathbf{\Phi} = diag[e^{-j2\pi kl/K}]_{k=0\ldots K-1} \tag{5.11}$$

It is easier to express (5.10) with an extended matrix $\mathbf{\Delta}(n)$ to see how the received vector $Y(n)$ depends on the channel impulse response for purposes of channel estimation

$$\mathbf{\Delta}(n) = [\mathbf{\Phi}^{-A}\mathbf{D}_\theta(n) \ldots \mathbf{\Phi}^{L-1-A}\mathbf{D}_\theta(n)] \tag{5.12}$$

$$\mathbf{h}(n) = [\mathbf{h}_{-A}\mathbf{h}_{-A+1} \ldots \mathbf{h}_{L-A-1}] \tag{5.13}$$

$$\mathbf{Y}(n) = \mathbf{\Delta}(n)\mathbf{h}(n) + \mathbf{Z}(n) \tag{5.14}$$

If all the data symbols are known, the LS channel estimate can be obtained as

$$\widehat{\mathbf{h}}(n) = [\mathbf{\Delta}_k'(n)\mathbf{\Delta}_k(n)]^{-1}\,\mathbf{\Delta}'(n)\mathbf{Y}(n) \tag{5.15}$$

Variations on the construction of the matrix $\mathbf{\Delta}(n)$ are available in [2] as long as adaptive alternatives which don't require a matrix inversion. After having estimated the channel, we can perform an FFT, then equalize the symbols thanks to (5.2).

Channel sparsing

The advantage of doing the channel estimation on time domain is that it is supposed than fewer than K coefficients are sufficient for representing the CIR. Empirical observations of the SPACE'08 experiment conditions show that the channel has a CIR of about 4 ms which translates to 160 samples knowing the sampling rate of the system. If an estimation on the frequency domain had to be done, K coefficients would have to be calculated.
A part from improving on computing time, channel sparsing can also be done. The estimated CIR will contain noise and so will do the final demodulations. To reduce the noise power, taps shorter in magnitude than a certain thresold can be eliminated. They are considered to contain only noise, so eliminating them keeps only the most important ones, smoothing the frequency response.

Channel estimated length

Note that in order for a solution to exist, the necessary condition is that $K \geq M_t L$. This condition can be interpreted in two ways: (1) for a given number of carriers K, at most K/M_t channel coefficients can be estimated; and (2) for a given channel span L, at least $M_t L$ observations are needed. If fewer than K observations are used, as would be the case in a block-oriented approach, the those rows of the matrices $\mathbf{Y}(n)$ and $\mathbf{\Delta}(n)$ that correspond to the pilot carriers will be isolated from the expression (5.15) to form a reduced set of ($P = M_t L$) observations. The underlying data symbols (M_t per observation) have to be known. If all the data symbols can be known, as it is the case in a decision-directed approach, it is advantageous to utilize all K observations instead of $M_t L$ only.

Chapter 6

ICI Algorithms

OFDM assumptions conform to a fixed CIR within a symbol block. If spacing between subcarriers is too short (long symbol block time) channel impulse response can change substantially within that period of time. Intercarrier interference is then produced because of the orthogonality loss between subcarriers. Specific demodulation techniques are needed to deal with this effect; nevertheless, vast literature is found on this topic. Equalization algorithms by means of matrix inversion are found in, [7], [8], [9], [10], or by means of adaptive equalization, [11]. In addition to these references, Taylor approximation of the channel variation is found on [12]. The system model described in section 2.2 is a valid model but it would be easier if we are able to express it in a matrix form

$$\mathbf{y}(n) = \mathbf{H}(n)\mathbf{d}(n) + \mathbf{n}(n) \tag{6.1}$$

Defining $\mathbf{y}(n) = [y_0(n), y_1(n) \dots y_{K-1}(n)]^T$ the symbols received in each subband and $\mathbf{d}(n) = [d_0(n), d_1(n) \dots d_{K-1}(n)]$ the symbols sent in each subband. The vector $\mathbf{n}(n)$ contains the noise and the channel matrix is defined as:

$$\mathbf{H}(n) = \begin{bmatrix} H_{0,0}(n) & H_{0,1}(n) & \dots & H_{0,K-1}(n) \\ H_{1,0}(n) & H_{1,1}(n) & & \\ \vdots & & \ddots & \\ H_{K-1,0}(n) & & & H_{K-1,K-1}(n) \end{bmatrix} \tag{6.2}$$

Where the channel coefficient $H_{i,j}(n)$ is specifying interference from subcarrier j to subcarrier i. Once stablished the new channel model, a simple LS solution can be performed to find the transmitted data symbols:

$$\widehat{\mathbf{d}}(n) = [\mathbf{H}'(n)\mathbf{H}(n)]^{-1}\mathbf{H}'(n)\mathbf{y}(n) \tag{6.3}$$

In many systems, though, the channel matrix $\mathbf{H}(n)$ is considered to be banded. That is, only a few adjacent subcarriers are affecting the current examined symbol like shown in figure 6.1. This specific structure is advantageous because the inverse of such matrices can be computed faster than general propertyless matrices [10]. Knowing that an OFDM system can have a large number of subcarriers and thus a large channel matrix, this simplification is of great computational savings.

Although the model is pretty simple, the main challenge of the algorithms is to estimate the channel. Several are proposed, like pilot aided channel estimation, adaptive algorithms like a Frequency Domain Decision Feedback Equalizer (FD-DFE) or modeling the channel variation with a Taylor approximation for example. An overview of the demodulations techniques and their results will be explained here.

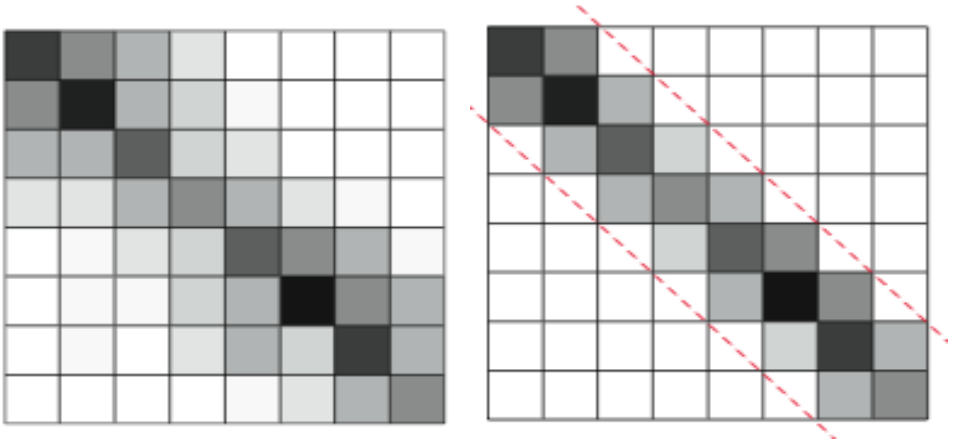

Figure 6.1: Typical channel matrix for an ICI problem. Dark points mean highest coefficients

6.1 Estimating the channel matrix

Pilot aided estimation

As in many OFDM systems, channel estimation can be performed by means of known received data, that is pilot tones. There are many alternatives about pilot distribution within OFDM blocks

- Use an OFDM to send all pilot symbols, sacrificing all the bit rate but obtaining a better channel approximation. The pilot block is repeated with a certain spacing depending on the application and block in between are all data. This scheme is used in [1] for an adaptive channel estimation
- Reserve certain tones in each block for pilot allocation. The tones normally are equally spaced because less computational complexity will be required when demodulating.

Although channel estimation neglecting ICI can be somewhat easy with pilots, when taking into account the ICI terms, the process gets complicated. There is a vast number of techniques, some of them are commented here

- Othogonal matching pursuit The algorithm is described in [13] and it basically tries to find the best fit of the matrix channel into the signal subspace. The algorithm assumes a Doppler spread model,[14], and then it calculates the channel paths iteratively until the estimation and the observations are similar enough (the metric used to compute the error goes below a predefined threshold).

- 2-D Polynomial Surface Channel Estimator In [7] the channel is modeled as a mathematical smooth surface within a certain time-frequency region. In a nutshell, pilots are inserted equally spaced in time and frequency; that is very p_t frames K/p_f pilots are inserted for estimation purposes. The channel, for a block index n and sample l for the frequency index k ios modeled as

$$H_{k,l}^n = \sum_{i+j \leq p} c_{i,j} \cdot k^i \left(n((N+T_g)+l\right)^j = \mathbf{c}^H \mathbf{q}_{k,l}^n \tag{6.4}$$

To find the coefficients **c** a minimization algorithm is run using the known data. Although this estimation can be done in the frequency domain, time domain estimation is much more efficient because, usually, the length of the CIR is much less than the number of subcarriers. The previous equation then transforms into the time domain, but the minimization process is kept similar.

- **Basis Expansion Model** The basic idea of this algorithm is to express each channel path as a linear combination of deterministic time-varying functions defined over a limited time span. Each channel path evolution can be expressed as $\mathbf{g}_l = [h_{0,l}, \cdots, h_{N-1,l}]$ with N the number of samples received. The basis expansion model (BEM) express the channel as

$$\mathbf{g}_l = \mathbf{\Xi}\eta_i = [\xi_0, \cdots, \xi_Q][\eta_{l,0}, \cdots, \eta_{l,Q}]^T \tag{6.5}$$

Like the other algorithms, to find the path evolution, a minimization algorithm is run leading to an MMSE estimate for the coefficients $\eta_{i,j}$ of the basis functions ξ_j for a basis of length Q. A popular choice of the basis functions is represented by complex exponentials, because they are orthonormal by definition and the final channel matrix **H** can be banded although other choices are possible.

Adaptive Frequency Channel Estimator

An effective way to estimate the channel coefficients is by means of a gradient algorithm [11]. From the a priori known symbols $d_k(n)$, an error signal is formed

$$E_k(n) = y_k(n) - \sum_{m=-I}^{I} \widehat{H}_{k,k+m}(n) d_k(n) \tag{6.6}$$

And P is the number of subcarriers neighbors that are considered to be interfering. From this error signal, a gradient algorithm is constructed, namely LMR or RLS to iterate along all subcarriers in the following manner:

$$\widehat{\mathbf{H}}_k(n) = \widehat{\mathbf{H}}_{k-1}(n) + \mathbf{\Gamma}(n)\epsilon_k(n) \tag{6.7}$$

Defining

$$\begin{aligned} \widehat{\mathbf{H}}_k(n) &= [\widehat{H}_{k,k-I}(n), \ldots, \widehat{H}_{k,k+I}]^T \\ \epsilon_k(n) &= [E_k(n)d^*_{k-I}(n), \ldots, E_k(n)d^*_{k+I}(n)]^T \\ \mathbf{\Gamma}(n) &= diag(\gamma_{-I}(n), \ldots, \gamma_{+I}(n)) \end{aligned}$$

Where $\mathbf{\Gamma}$ represent the gradient coefficients and its values depend of the type of algorithm used. So, it is clear that all the K symbols should be known. This means that either we can use pilot signals (which is not of interest) or we can make tentative decisions before iterating. Depending on the correctness of the a priori decisions, the channel matrix will be accurately estimated. Simplification of this algorithm implies to restrict the number of interfering subcarriers, being the simplest case with only two interfering neighbors ($I = 1$)

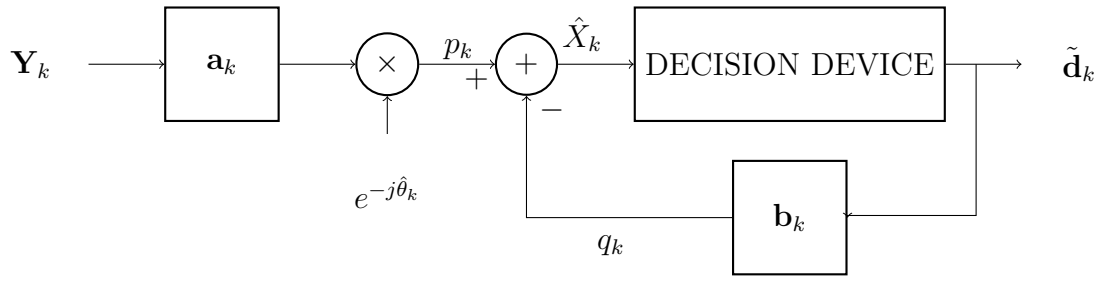

Figure 6.2: Scheme of a Frequency Domain DFE

Frequency Domain - Decision Feedback Equalizer

A decision-feedback equalizer is a nonlinear equalizer that contains a forward filter and a feedback filter. Unlike the linear equalizer, the DFE doesn't have to estimate the explicit ICI coefficients. In the classical way, the DFE was widely used for intersymbol interference (ISI) cancellation. In OFDM, information is sent among independent channels, so ICI can be treated as ISI but in a causal and anticausal way. In ISI approaches, only symbols that were sent before would affect the current decision, but in the frequency domain and ICI, the influence comes from the higher and the lower subcarriers. See the scheme proposed in figure 6.2 and the corresponding explanation for more details.

Inputs of the DFE are vectors formed by $2I + 1$ elements corresponding to the ICI coefficients that must be taken into account. Normally, as in the linear equalizers, $I = 1$ so the vectors have 3 elements. The inputs are filteres and then are multiplied by the phase corresponding to the subcarrier with index k. The output of the decision device is also a vector of $2I + 1$ elements which come from previous decisions. A filtering of this output subtracted to the filtered phase-corrected input for the new input to the next decision module. For each iteration, the optimal coefficients conditioned to the phase estimate are:

$$\mathbf{w}_k^{opt} = \left(E\left\{\mathbf{U}_k\mathbf{U}_k'\right\}\right)^{-1} E\left\{\mathbf{U}_k d_k^*\right\} \tag{6.8}$$

where

$$\mathbf{w}_k^{opt} = \begin{bmatrix}\mathbf{a}_k^{opt} & \mathbf{b}_k^{opt}\end{bmatrix} \tag{6.9}$$

and

$$\mathbf{U}_k = \begin{bmatrix}\mathbf{Y}_k e^{-j\widehat{\theta}_k} & \tilde{\mathbf{d}}_k\end{bmatrix} \tag{6.10}$$

This process is repeated for all the subcarrier indexes and the coefficients are updated using RLS or LMS. Phase tracking is implemented using a second-order locked loop. In the system, the phase is modeled as

$$\theta_k = \theta_0 + a2\pi f_k T' \tag{6.11}$$

With usually $\theta_0 = 0$. From the MSE solution found for the DFE, the recursion describing the phase tracking is done with

$$\hat{\theta}_{k+1} = \hat{\theta}_k + G_1\psi_k + G_2\sum_{i=0}^{k}\psi_k \tag{6.12}$$

With G_1 and G_2 the step sizes of the loop. Normally, $G_2 = G_1/10$ and G_1 is tunned manually observing experiment results. The gradient estimate ψ_k is computed as

$$\psi_k = \Im\left\{p_k(p_k + e_k)^*\right\} \tag{6.13}$$

Taylor approximation

The approach used is to consider a linear channel tap variation within each OFDM block. That means that the channel has to be estimated before and after the demodulation of the block. The algorithm runs in the time domain, so only the CIR has to be estimated. As the CIR is related to the frequency response via a Fourier relationship, estimating the first is equivalent to have the latter. Going to the channel response domain can be advantageous if we want to apply channel sparsing, hence, noise variance can be reduced. The channel estimate of the previous block is always available, so the challenge is to obtain the next channel estimation without the use of pilots. To accomplish this, algorithm in [1] is executed and a channel esimation is calculated after making the final decisions. We then have the two channel estimates that can help to calculate the time variation.
Let's define the channel as a variant-time vector inside a block, from the first sample, $n = 0$,to the sample $n = N - 1$

$$\mathbf{h_0} = [h_{0,0}, h_{0,1}, \ldots, h_{0,L-1}]^T \quad \text{CIR in the start of the block} \tag{6.14}$$

$$\mathbf{h_{N-1}} = [h_{N-1,0}, h_{N-1,1}, \ldots, h_{N-1,L-1}]^T \quad \text{CIR at the end of the block} \tag{6.15}$$

From these two variables we can consider the CIR to vary inside a block as:

$$\mathbf{h}_k = \mathbf{h}_0 + k \times \frac{\mathbf{h_0} - \mathbf{h_{N-1}}}{N-1} = \mathbf{h}_0 + k \times \frac{\mathbf{\Delta h}}{N-1} \tag{6.16}$$

Basically, in each sample, the channel varies an amount of $\frac{\mathbf{\Delta h}}{N-1}$. So, if the received signal can be expressed as:

$$\mathcal{Y}_n = \sum_{l=0}^{L-1} h_{n,l} s_{|n-l|} + \tilde{n}_n \tag{6.17}$$

Where s_n is the sample n of the sent signal which is a common modulated OFDM block. Overlap add is used to convert linear convolution into circular convolution. The signal received is, in matrix notation:

$$\mathcal{Y} = \mathcal{H}\mathbf{s} + \tilde{\mathbf{n}} = \begin{bmatrix} h_{0,0} & h_{0,N-1} & \ldots & h_{0,1} \\ h_{1,1} & h_{1,0} & \ldots & h_{1,2} \\ h_{2,2} & \vdots & \ddots & \vdots \\ h_{N-1,N-1} & h_{N-1,N-2} & \ldots & h_{N-1,0} \end{bmatrix} \times \begin{bmatrix} s_0 \\ s_1 \\ \vdots \\ s_{N-1} \end{bmatrix} + \tilde{\mathbf{n}} \tag{6.18}$$

The vector $\tilde{\mathbf{n}}$ contains noise. As the channel is varying, we can relate the $\mathbf{H}$ matrix coefficients by the linear relationship in equation (6.18)

$$\mathcal{H} = \begin{bmatrix} h_{0,0} & h_{0,N-1} & \ldots & h_{0,1} \\ h_{0,1} & h_{0,0} & \ldots & h_{0,2} \\ \vdots & \vdots & \ddots & \vdots \\ h_{0,N-1} & h_{0,N-2} & \ldots & h_{0,0} \end{bmatrix} + \frac{1}{N-1} diag(0, 1, 2, \ldots, N-1) \times \begin{bmatrix} \Delta h_0 & \Delta h_{N-1} & \ldots & \Delta h_1 \\ \Delta h_1 & \Delta h_0 & \ldots & \Delta h_2 \\ \vdots & \vdots & \ddots & \vdots \\ \Delta h_{N-1} & \Delta h_{N-2} & \ldots & \Delta h_0 \end{bmatrix} \tag{6.19}$$

To simplify notation we will express the channel as

$$\mathcal{H} = \mathbf{A}_0 + \frac{1}{N-1}\mathbf{D}\mathbf{A}_1 \tag{6.20}$$

From equations (6.19) and (6.20) we can see that the matrices $\mathbf{A}_0$ and $\mathbf{A}_1$ are Toeplitz. When receiving the signal, an FFT operation is performed. $\mathbf{W}$ will be used to denote

the inverse Fourier transform so, $\mathbf{W^H}$ denotes the Fourier transform itself. Knowing that the sent signal is $\mathbf{s} = \mathbf{Wd}$, the received signal becomes, in the frequency domain

$$\mathbf{y} = \mathbf{W}'\mathcal{H}\mathbf{W}\mathbf{s} = \mathbf{W}'(\mathbf{A}_0 + \frac{1}{N-1}\mathbf{D}\mathbf{A}_1)\mathbf{W}\mathbf{d} + \mathbf{n} \tag{6.21}$$

The challenge is to find the Fourier transform for the matrices A_0 and A_1 separately to simplify the process. As said before, it's Toeplitz nature will define its structure

$$\mathbf{W}'(\mathbf{A}_0 + \frac{1}{N-1}\mathbf{D}\mathbf{A}_1)\mathbf{W} = (\mathbf{W}'\mathbf{A}_0\mathbf{W}) + \frac{1}{N-1}(\mathbf{W}'\mathbf{D}\mathbf{W})(\mathbf{W}'\mathbf{A}_1\mathbf{W}) \tag{6.22}$$

$$\mathbf{A}_0^f = \mathbf{W}'\mathbf{A}_0\mathbf{W} \tag{6.23}$$

$$\mathbf{A}_1^f = \mathbf{W}'\mathbf{A}_1\mathbf{W} \tag{6.24}$$

$$\mathbf{D}^f = \mathbf{W}'\mathbf{D}\mathbf{W} \tag{6.25}$$

The received signal becomes:

$$\mathbf{y} = (\mathbf{A}_0^f + \frac{1}{N-1}\mathbf{D}^f\mathbf{A}_1^f)\mathbf{d} + \mathbf{n} = \mathbf{H}\mathbf{d} + \mathbf{n} \tag{6.26}$$

The problem resides in finding the expressions of matrices $\mathbf{A'}_0$, $\mathbf{A}'_1$ and $\mathbf{D}'$. The latter has no difficulties since it is a fixed matrix and can be precalculated before the demodulation process begins. As a result, $\mathbf{D}'$ is a Toeplitz matrix whose first row elements are the IFFT of the diagonal elements of $\mathbf{D}$.
$\mathbf{A'}_0$ is a little trickier to find, but after playing with the properties of $\mathbf{A}_0$ we can show that it is a diagonal matrix whose elements are the Fourier transform of $\mathbf{h}_0$. Equivalently, $\mathbf{A'}_1$ is a diagonal matrix whose elements are the transform of the $\mathbf{\Delta h}$ vector.
Once found the transforms of the previous matrices and calculated the expression for $\mathbf{H}$ and MMSE estimate is constructed

$$\widehat{\mathbf{d}} = (\mathbf{H}'\mathbf{H})^{-1}\mathbf{H}'\mathbf{y} \tag{6.27}$$

Matrix $\mathbf{H}$ will be typically banded, being the coefficients of the main diagonal more important than the others.

6.2 Inverting the channel matrix

All along this section, several methods for estimate the channel matrix are considered. Although estimation is the most difficult part theoretically, the inversion of large matrices iand the amount of operations spent on doing so is what practical systems need to do fast. The ICI channel matrix is of dimensions $K \times K$, quite big if an inversion is required. Since the MMSE solution of the demodulated symbols computes an inverse of this size, several approaches are possible to make it simpler.

LDL^H Factorization

One of the forms of making the process faster, is to perform the inversion in two different parts [10]. As a first step, the Channel matrix is truncated and only its main P diagonals are only considered. As shown in equation (6.3) the solution is

$$\widehat{\mathbf{d}}(n) = [\hat{\mathbf{H}}'(n)\hat{\mathbf{H}}(n)]^{-1}\hat{\mathbf{H}}'(n)\mathbf{y}(n) \tag{6.28}$$

Where $\hat{\mathbf{H}}(n)$ is the Q-diagonal approximation of $\mathbf{H}(n)$. If we consider the matrix $\mathbf{M}$(n) $= \hat{\mathbf{H}}'(n)\hat{\mathbf{H}}(n)$. This matrix has a band of $2Q$ either upper or lower. If an inversion of this matrix is desired, a Cholesky decomposition or the LDL^H factorization can be computed. Here are the procedures for this algorithm

1. Construct the Q-diagonal matrix $\hat{\mathbf{H}}(n)$ from the original $\mathbf{H}(n)$
2. Construct the $\mathbf{M}$ matrix
3. Perform a LDL^H factorization of $\mathbf{M} = \mathbf{LDL}^H$, where $\mathbf{D}$ is the diagonal and the triangular matrix $\mathbf{L}$ has lower bandwidth $2Q$
4. Solve the system.
   - Solve $\mathbf{f} = \mathbf{L}^{-1}\mathbf{y}(n)$ which is efficient because of the properties of $\mathbf{L}$
   - Solve $\mathbf{g} = \mathbf{D}^{-1}\mathbf{f}$ which is trivial begin $\mathbf{D}$ diagonal
   - Solve $\mathbf{q} = \mathbf{L}^{-H}\mathbf{g}$
5. Compute the final symbol estimate $\widehat{\mathbf{d}}(n) = \hat{\mathbf{H}}(n)\mathbf{q}$

The computation complexity then reduces proportional to the number of diagonals Q square considered. Usually, $Q = 1, 2$ so the matrix inversion operations, instead of being propotionals to K^3, are only proportional to K.

LSQR Iterative method

The LSQR iterative method uses a QR decomposition and then solves a bidiagonlization least squares problem [15], [16]. The equation are proposed in a similar manner:

$$(\mathbf{H}'\mathbf{H})^{-1}\widehat{\mathbf{d}} = \mathbf{H}'\mathbf{y} \tag{6.29}$$

The algorithm can be summarized as follows

1. Initialization

$$\alpha_1 = \|\mathbf{H}'\mathbf{y}\|, \quad \beta_1 = \|\mathbf{y}\|, \quad \mathbf{u}_1 = \frac{\mathbf{y}}{\beta_1}, \quad \mathbf{v}_1 = \frac{\mathbf{H}'\mathbf{y}}{\alpha_1}$$

2. Recursion

$$\begin{aligned} \alpha_{i+1} &= \|\mathbf{H}'\mathbf{u}_i - \beta_i\mathbf{v}_i\| \\ \beta_{i+1} &= \|\mathbf{H}'\mathbf{v}_i - \alpha_i\mathbf{u}_i\| \\ \mathbf{u}_{i+1} &= \frac{1}{\beta_{i+1}}\left(\mathbf{H}'\mathbf{v}_i - \alpha_i\mathbf{u}_i\right) \\ \mathbf{v}_{i+1} &= \frac{1}{\alpha_{i+1}}\left(\mathbf{H}'\mathbf{u}_i - \beta_i\mathbf{v}_i\right) \end{aligned}$$

The main advantage of the process is that is an iterative and it can be stopped at any iteration. Theoretically, it is terminated when either one of the constants, α_i, β_i is zero. Practically, the process is run until one of the values falls below a certain threshold. After finding the values, a minimization error is computed and from the vectors $\mathbf{v}_i$ and the solution found from the minimization, the original data $\widehat{\mathbf{d}}$ is retrieved.
As seen, no matrix inversions are required at all, so the computational cost of this algorithm is chosen with the number of iterations. In practice this number is between 10 and 20 making the algorithm run quicker as the normal inversion method.

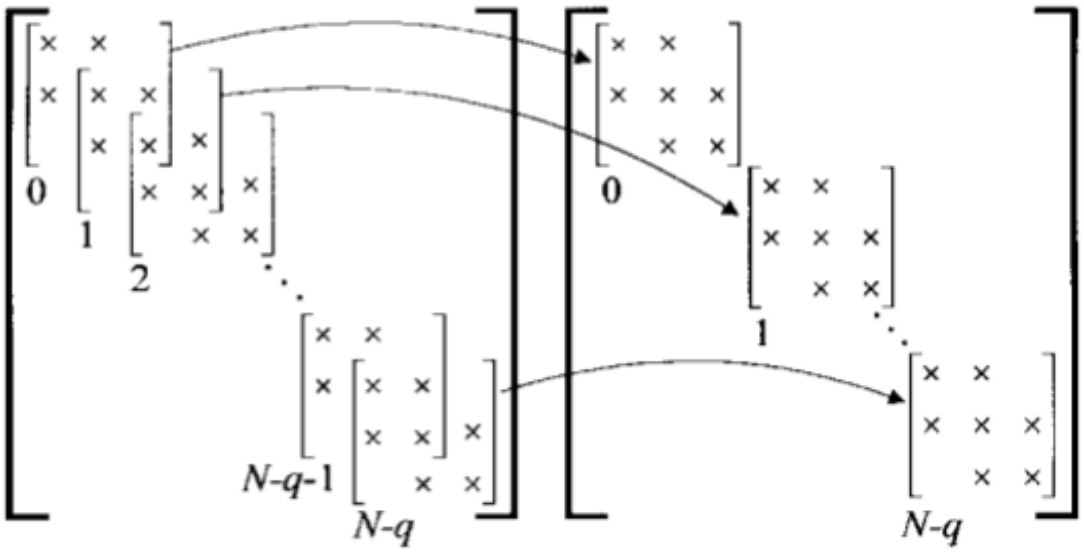

Figure 6.3: Example of decoupling the diagonal of the channel matrix

Matrix Decoupling

This mehtod is a simple idea from which the large matrix to be inverted is decoupled into several, smaller matrices, to be inverted. Figure 6.3 shows one of the possible alternatives to achieve this. By block-diagonalizing the matrix, its inversion its much simpler and it only requires a complexity according to the number of Q diagonals chosen. Instead of making one large $K \times K$ which requires a time proportional to K^3, K inversions of $(2Q+1) \times (2Q+1)$ are performed reducing considerably the computation complexity by orders of magnitude.

Jacobi Stationary Iterative Method

This is also an iterative method for solving sparse matrix inversions. As the channel matrix $\mathbf{H}(n)$ is sparse if only the main diagonals are considered, then this method can be applied. It resumes on the following

1. Initialization A first initial symbol estimation, neglecting ICI

$$\widehat{\mathbf{d}}_0 = \left\{ \frac{y_0}{H_{0,0}}, \ldots, \frac{y_{K-1}}{H_{K-1,K-1}} \right\}$$

2. Iteration

$$\widehat{\mathbf{d}}_i = \widehat{\mathbf{d}}_0 - \mathbf{K^{-1}}(\mathbf{H} - \mathbf{K})\widehat{\mathbf{d}}_{i-1}$$

   Where $\mathbf{K}$ is a diagonal matrix and it is defined as $K = \text{diag}\,(H_{0,0}, \ldots, H_{K-1,K-1})$ so its inverse its symply the inverse of the diagonal coefficients. If the channel matrix is sparse, this method shows that after a reduced number of iterations, mainly 2 or 3, the estimates converge and more iterations do not show any substantial improvement on the BER.

Matrix Simplification

This technique was tried with algorithm in [12]. The point is to observe that the ICI coefficients of the adjacent subcarriers can be, in typical cases, $10dB$ in amplitude below the corresponding coefficient. That is $H^{dB}_{k,k\pm1} + 10dB = H^{dB}_{k,k}$. Assuming this result, to compute the LS estimate, the following approximation can be done:

$$\left(\hat{\mathbf{H}}'(n)\hat{\mathbf{H}}(n)\right)^{-1} \approx \text{diag}\left(\frac{1}{\sum_{k=0}^{K-1}\|H_{0,k}\|^2}, \ldots, \frac{1}{\sum_{k=0}^{K-1}\|H_{K-1,k}\|^2}\right) \tag{6.30}$$

Which is simply a truncation of the multiplication of the left hand side of the equation. Empirical results show that a difference of 30dB is usually found between the main and the upper diagonal, so truncation can be performed without observing any degradation on BER. Therefore, the final solution is

$$\widehat{\mathbf{d}}(n) = \text{diag}\left(\frac{1}{\sum_{k=0}^{K-1}\|H_{0,k}\|^2}, \ldots, \frac{1}{\sum_{k=0}^{K-1}\|H_{K-1,k}\|^2}\right)\hat{\mathbf{H}}'(n)\mathbf{y}(n) \tag{6.31}$$

Which doeas not require any matrix inversion.

Part III

Results and Conclusions

Chapter 7

Results on experimental data

7.1 MIMO

System description

The transmitted signals were of the zero-padded OFDM type, given by

$$\begin{aligned} s(t) &= Re\{u(t)e^{j2\pi f_0 t}\} \\ u(t) &= \sum_{k=0}^{K-1} d_k(n)g(t-nT')e^{j2\pi k\Delta f(t-nT')} \end{aligned} \tag{7.1}$$

where $g(t)$ is a unit-amplitude rectangular pulse of duration T, $T' = T + T_g$ is the signaling interval that includes the multipath guard time T_g, f_0 is the lowest carrier frequency, $\Delta f = 1/T$ is the subcarrier spacing, K is the number of subcarriers, and $d_k(n)$ is the data sumbol transmitted on the k-th subcarrier during the n-th signaling interval. In the case of multiple transmitters, a different data stream, $d_k^t(n)$, $t = 1, \ldots M_T$, was used to modulate each of the M_T transmitted signals.

The experiment, called the Surface Processes Acoustic Communications Experiment (SPACE), was conducted in October 2008, south of the island of Martha's Vineyard off the coast of New England. Figure 7.1 illustrates the deployment geometry. The transmit array (4 elements separated by 50 cm) and the receive array (12 elements, separated by 12 cm) were fixed vertically on the ocean floor.

The signals were transmitted around the clock over the course of 15 days. The same group of signals, lasting two minutes, was repeated every two hours. Each such group contained several OFDM frames with varying modulation parameters. Table 7.1 lists the signal parameters.

This selection of signal parameters corresponds to a large range of bandwidth efficiencies, 0.9-10.4 bps/Hz without coding, i.e. 0.1-1.6 bps/Hz with a 1/6 rate code. Not counting the code rate, the bandwidth efficiency is defined as the ratio of the bit rate to the bandwidth occupied,

$$\frac{R_b}{B} = M_T \frac{mK}{T'} = M_T \frac{m}{1 + T_g B/K} \tag{7.2}$$

where m is the number of bits per symbol, e.g. 3 if 8-PSK is used.

The environmental conditions during the experiment were varying, with periods of high wave activity. Figure 7.2 shows the wind speed, the wave height, and the wave period

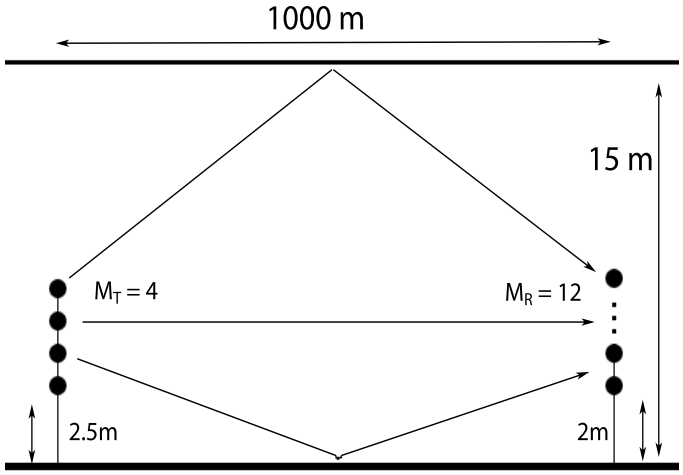

Figure 7.1: Geometry of the experiment.

bandwidth, B	10 kHz
lowest carrier frequency, f_0	8.25 kHz
sampling frequency, $f_s = 4B$	40 kHz
modulation method	QPSK, 8-PSK
coding	BCH (64,10)
symbols per frame, N_d	16384
number of carriers, K	128, 256, 512, 1024
carrier sacing, Δf [Hz]	78, 39, 19, 10
block duration, $T = 1/\Delta f$ [ms]	13, 26, 52, 105
blocks per frame, $N = N_d/K$	128, 64, 32, 16
guard time, T_g	16 ms

Table 7.1: Signal parameters.

observed during the experiment. As we will see in Sec.7.1, the system performance is related to some of these parameters; notably, it appears to deteriorate during the periods of increased wave height. The conjecture is that this behavior is caused by the fact that the CIR varies more rapidly during such periods. Other consequences of tough weather conditions would be more difficulties to track phases changes and some assumptions and simplifications that were proved to be successful in calm environments

The algorithm presented in chapter 5 was applied to the experimental data, to assess the performance in changing environmental conditions and derive general rules for the selection of system parameters. In particular, the goal was to identify the greatest number of carriers and transmit elements (greatest bandwidth efficiency) for which the performance meets some requirements. Example of received signals are shown in figure 7.3; clearly, the higher modulation level will be more error-likely because, in equal noise conditions, bad decisions will be made caused by the closeness of the decision boundaries.

Figure 7.4 shows an example of a channel response recorded during the experiment. Typically, the delay spread was below 10 ms, and $L = 128$ taps were chosen to capture the CIR (this corresponds to $128/B = 13$ ms). The algorithm was initiated using this value,

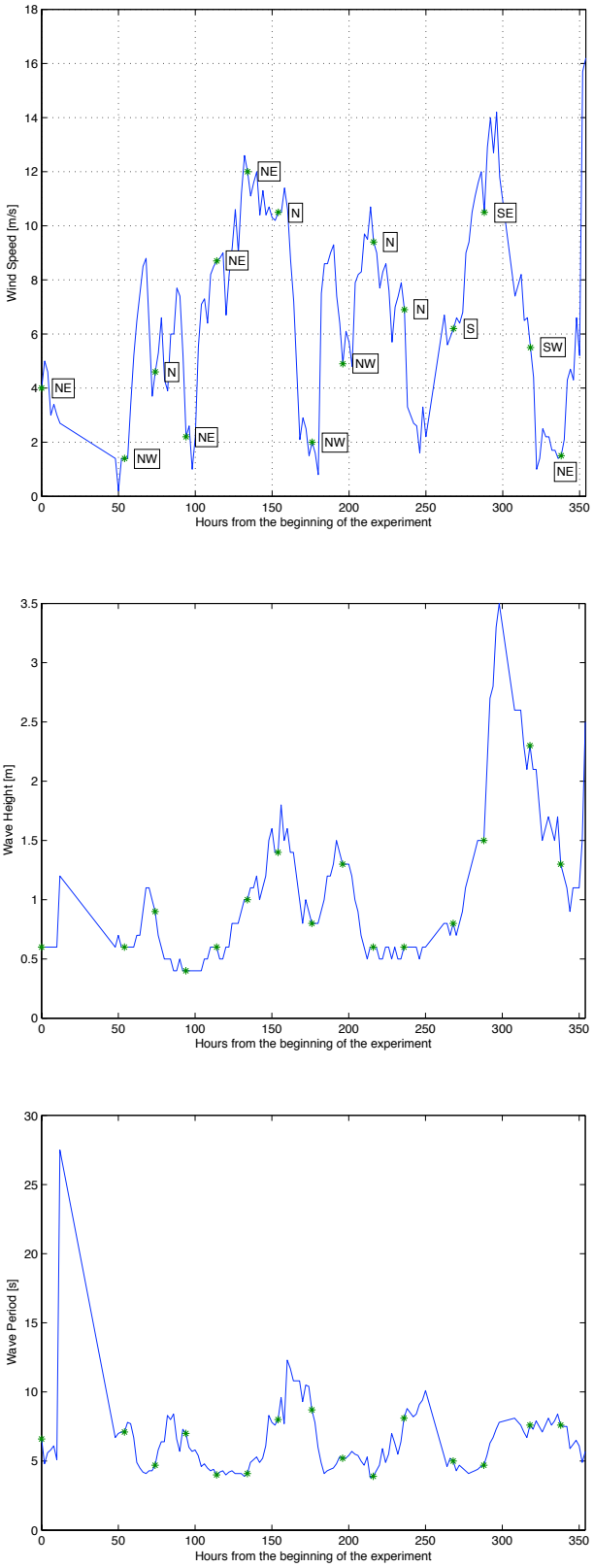

Figure 7.2: Wind speed with the wind direction indicated, wave height and wave period during the experiment. Stars mark the exact points in time when OFDM signals were recorded.

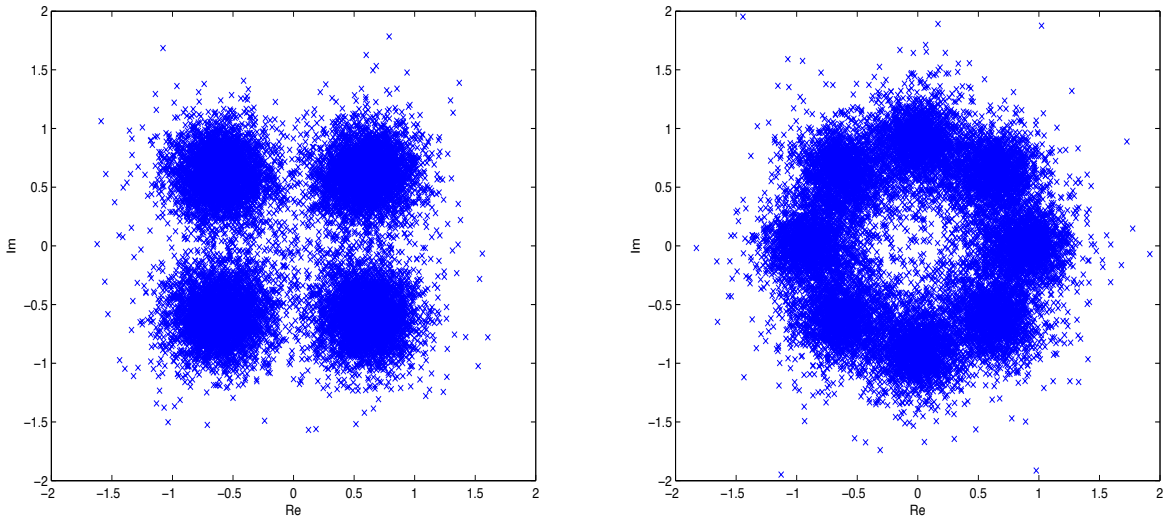

Figure 7.3: Scatter plot for received QPSK and 8-PSK signals

and further sparsing was performed on-line. Depending on the time of transmission, the average number of channel coefficients kept was between 60 and 120, section **??** will explain the details on channel sparsing. The channel tracking parameter μ was experimentally determined for each (M_T, K) configuration, and kept the same throughout the experiment. No pilot subcarriers were used.

Channel sparsing

Channel sparsing is a good way to (a) reduce the computing time of the algorithm and (b) eliminate part of the noise captured by the channel estimation. However, parameters of this algorithm should be selected carefully if a good demodulation process is wanted. Excessive truncation of the CIR can lead to distortion, and a too much conservative parameter can lead to a noisy symbol input for decision.

Figure 7.5 shows four different estimated CIR with different thresholds. The first one, with no sparsing at all, captures all the possible noise in the receivers while the second, with a low threshold, cuts the CIR in such a way that the energy of the lower taps is lost. It should be found a good trade-off between these two cases, where the number of taps ignored are less important than the noise eliminated. This trade-off happens to be between threshold of about 20-40 depending on the case examined.

In figure 7.6, the evolution of the MSE and coefficients kept is presented. First of all, it should be noticed that the coefficients kept is a linear asymptotically increasing function with the threshold. In an ideal case (where tha channel consisted on infinite taps, including noise), as the threshold will approach infinity, the percentage of coefficient kept will be close to 100%. In a real case, where the length of the channel is limited to L taps, this function saturates fast. A first approximation of the optimal threshold can be inferred from this graphic. Knowing the fact that noise taps will be all of the same magnitude, selecting a threshold corresponding to the left part of the funcion with maximum derivative will work as a first instance.

The best method, though, to assess the optimal coefficient is to plot the MSE and values in function of the sparsing threshold. We can see that there is a clear minimum. This

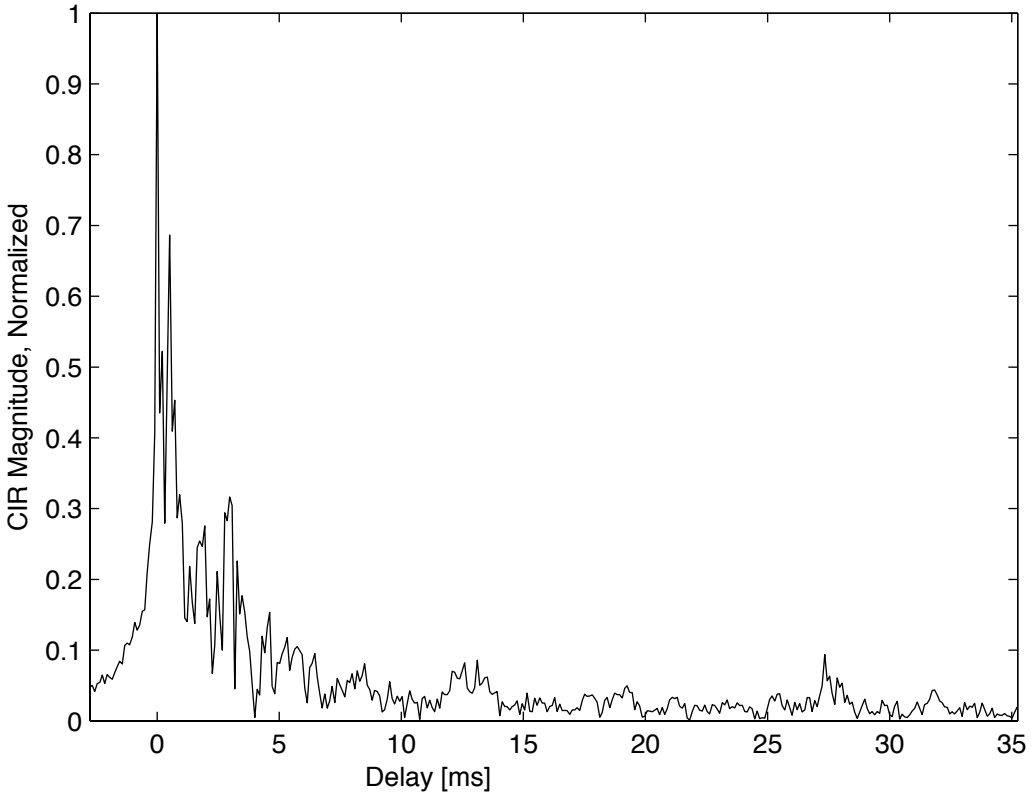

Figure 7.4: A typical channel impulse response.

behavior was observed in all the data sets and the values obtained were all around 20-40. Then, the receiver parameter established that a sparsing threshold of 30 would work offering the minimum possible MSE in average. This conclusions, somehow is correlated with the previous analysis and the figure 7.5.

Phase Tracking & Doppler factor

Phase tracking proved to be crucial for the performance of the algorithm. The algorithm offered better performance when more subcarriers were used. The explanation of this is because the estimation of the doppler factor is more accurate when more observations are possible as the noise variance is reduced when averaging, this effect can be shown on figure 7.7 were the phase of each the subcarriers is ploted for two different transmission with $K = 128, 1024$. The three colors represent three different transmissions being the blue the day with maximum wave height, the red the day with minimum, and the black being a random day with a wave height between the maximum and the minimum. As K lowers, phases become more drifty and noisy. Phase correction was performed non-uniformly because of the nature of the UWA channel. As stated in the previous section, the bandwidth of the system was 8-18kHz, clearly of wide-band nature. We can then perform an analysis on the estimated doppler factor and consequently, the phases obtained related by equation 4.5.

An intuitive analysis would say that the higher the wave height, the higher the phase

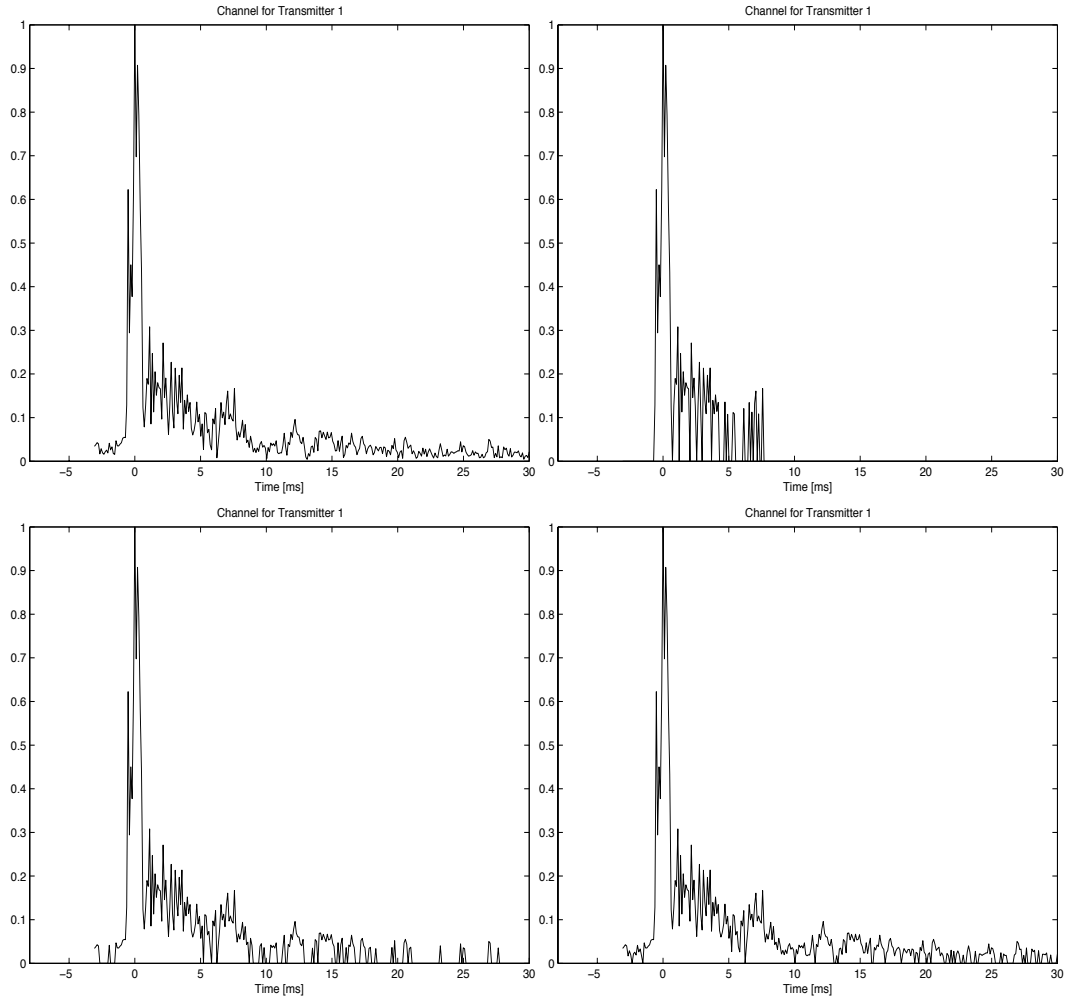

Figure 7.5: Channel Impulse Response estimated for a different number of threshold. From left to right and top to bottom: no sparsing, 10, 30, 60.

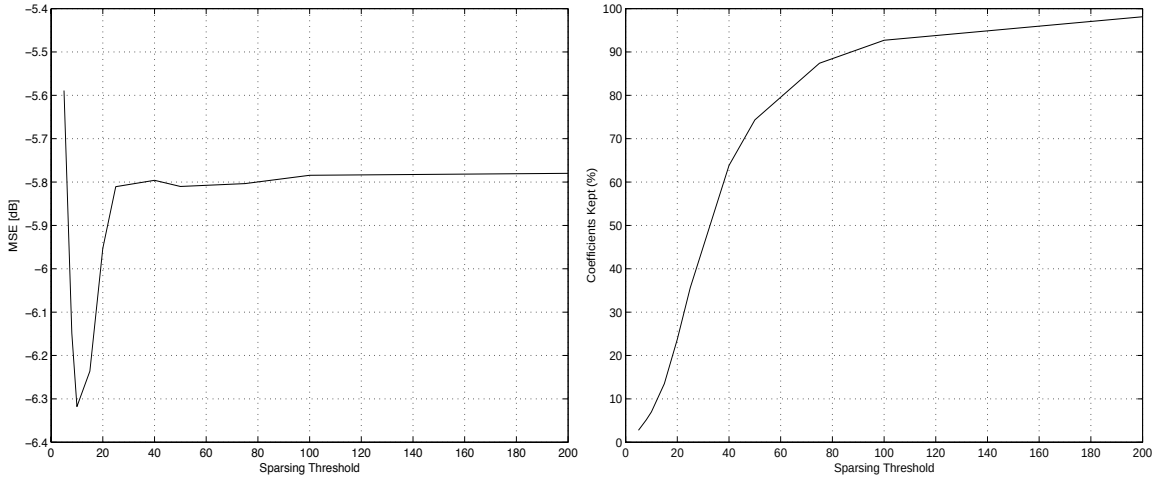

Figure 7.6: MSE and Coefficients kept (left to right) for a different number of sparsing thresholds

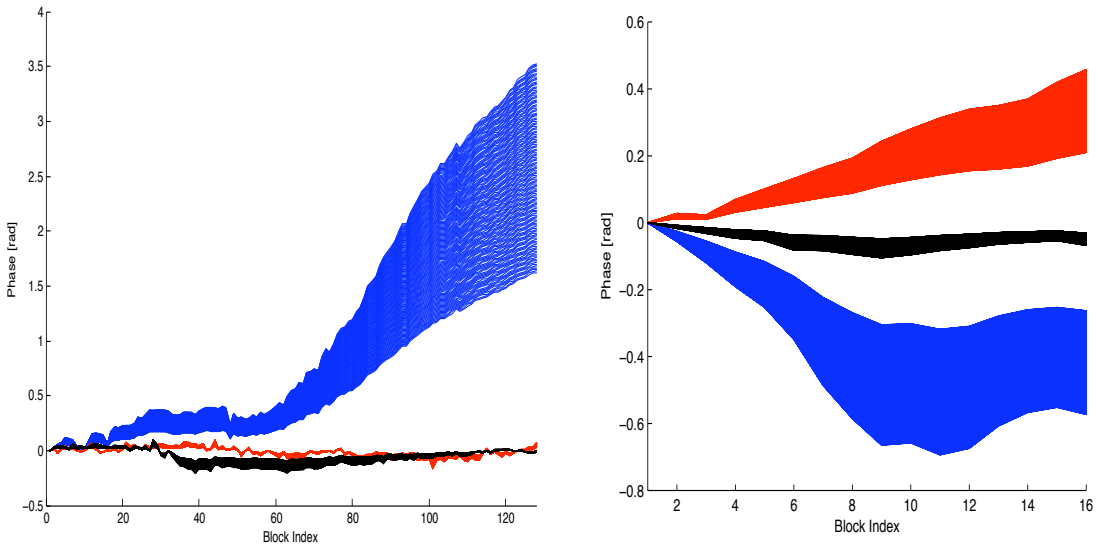

Figure 7.7: Phases of three experiments with 128 and 1024 subcarriers and 1 transmitter.

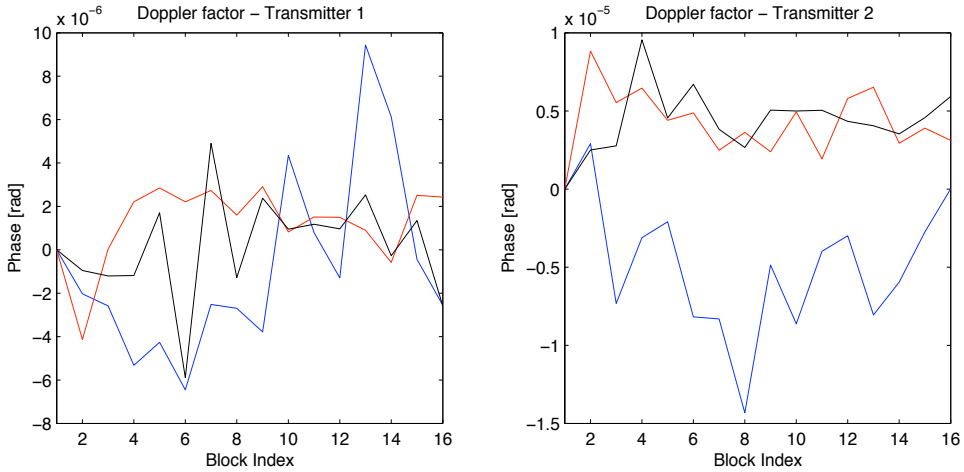

Figure 7.8: Doppler of three experiments with 1024 subcarriers and 1 transmitter

variation. Figure 7.7 reflects somehow this effect, making blue lines vary more than the red and black ones. A severe phase variation will indeed make errors more likely, and these errors will also be correlated with the wave height and other enviromental conditions. Conlusions on this will be detailed in section 7.1

A different factor for each of the transmitters was also vital for phase tracking. As shown in figures 7.9 with the phases and 7.8 with the corresponding doppler factors, shapes are completely different and one transmitter results to have a different doppler factor than the other. These results can be extended to more transmitters, but for the sake of brevity only results with two transmitters are presented. Some times it is possible to average between transmitters, but in this experiment, separated values had to be used.

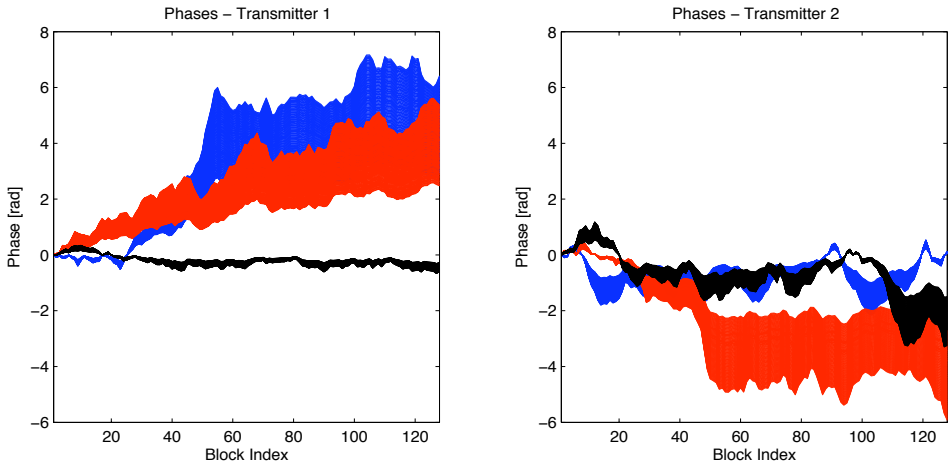

Figure 7.9: Phases of three experiments with 1024 subcarriers and 2 transmitters

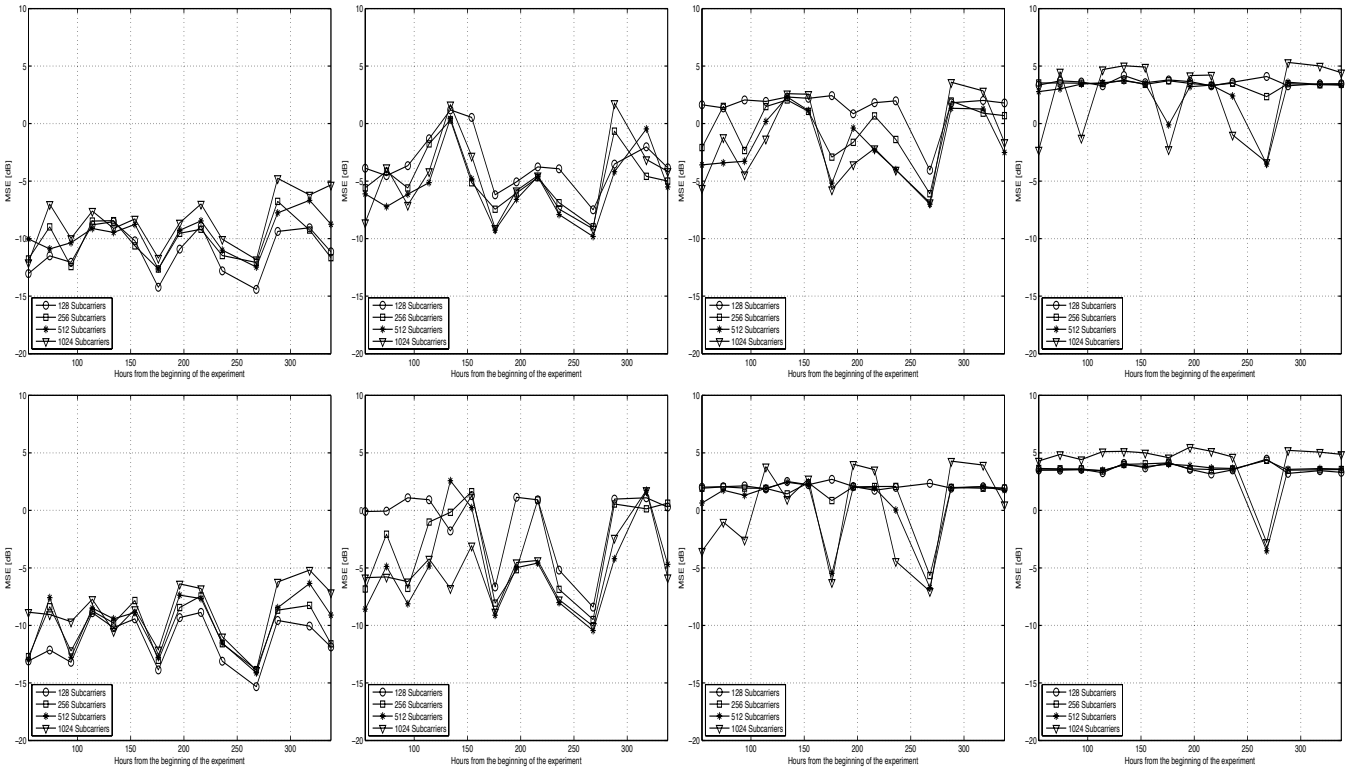

Figure 7.10: MSE for QPSK (top) and 8-PSK (bottom) for varying number of transmitters, M_T=1, 2, 3 and 4 from left to right.

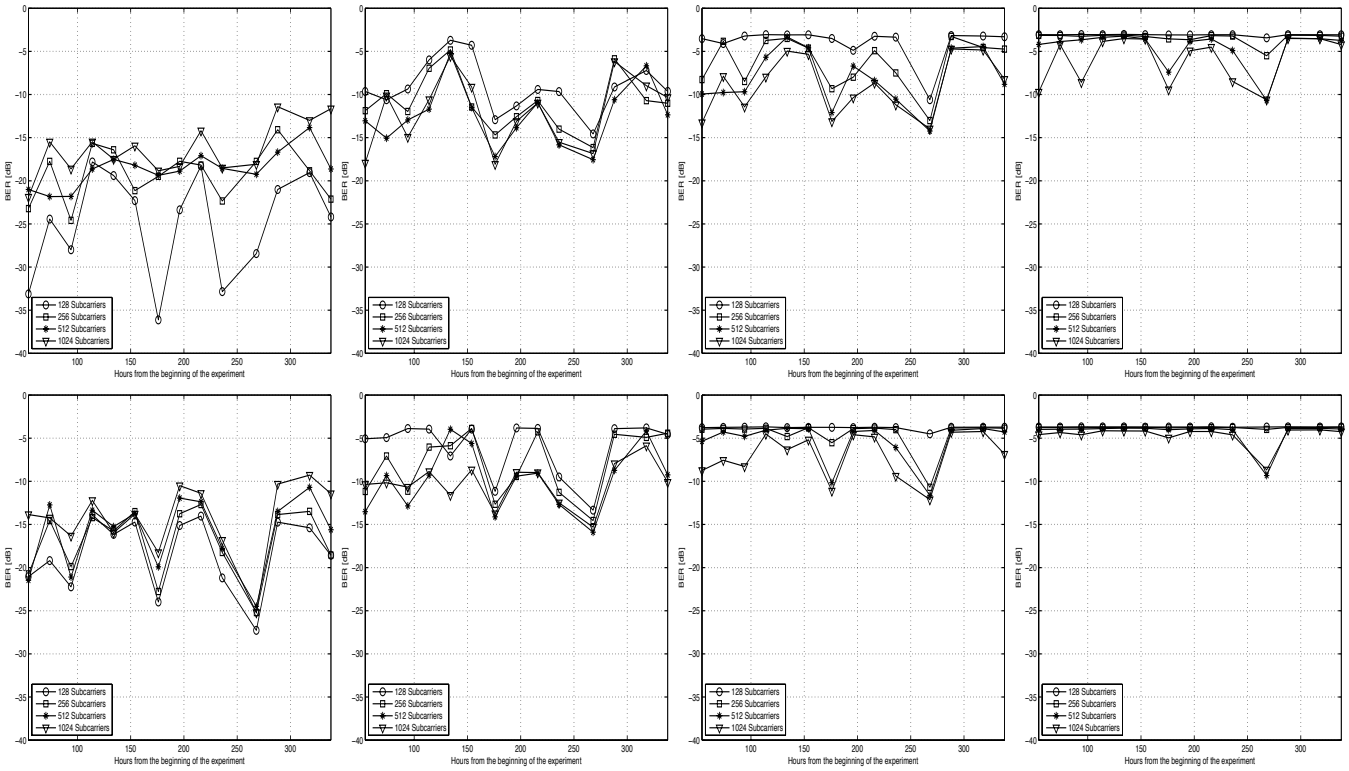

Figure 7.11: BER without coding for QPSK (top) and 8-PSK (bottom) for varying number of transmitters, M_T=1, 2, 3 and 4 from left to right.

MSE & BER

Focusing on the results for $M_T = 1$, we note that both modulation methods perform well. The performance degrades slightly as the number of carriers increases from 128 to 1024. This indicates that the system is not *limited* by the time variability of the channel at hand, although it is influenced by it. The uncoded BER varies following the same pattern as the MSE, but the coded BER stays zero throughout the measurements.

As the number of transmit elements increases, the performance deteriorates, since the same physical channel is now used to transmit multiple data streams, which generate cross-talk. With M_T=2, the deterioration is gradual, and the system manages to separate multiple channels. It is interesting to note that lower values of K experience higher loss, thus reversing the performance trend with K. The exact way in which this effect takes place is rather hard to judge, because there exists an inherent trade-off between the number of carriers K and the system performance: on the one hand, a greater K implies a longer block, and, hence, a more substantial channel variation that can hurt the system performance (by violating the time-invariance assumption and creating ICI); on the other hand, a greater K provides more observations for the decision-directed channel estimator, thus boosting its performance. From the viewpoint of bandwidth efficiency, it is of course advantageous to use the greatest possible number of subcarriers, and for the present experiment, we see that K=1024 is a good choice with M_T=2. Hence, this is a "win-win" situation, in which the bit rate is doubled by spatial multiplexing, while a large number of carriers (K=1024) provides efficient use of the multipath guard time without much compromise to the time-invariance assumption.

As M_T increases further, performance is lost in many instances. With M_T=3, lower

values of K are the first to experience a complete loss in performance, while the system with more carriers copes with the changing conditions, showing periods of varying performance that coincide with those observed at M_T=1 and 2. At M_T=4, the system fails.

Performance loss with increasing M_T is inevitable, as the task of MIMO channel estimation becomes increasingly difficult in the presence of increased cross-talk between the channels. In fact, MIMO channel estimation is conditioned on having the number of transmitters $M_T \leq K/L$, which ensures the existence of the estimate (**??**). Hence, as more transmitters are added, this condition eventually becomes violated specially with lower values of K.

From the viewpoint of bandwidth efficiency (7.2), this limit on the number of transmitters implies that

$$\frac{R}{B} \leq \frac{K^2}{LK + L^2} \text{ [symbols/sec/Hz]} \tag{7.3}$$

Hence, for a given multipath spread $L \sim BT_g$, bandwidth efficiency is ultimately limited by the number of carriers. Although the time variability of the channel prevents the use of an arbitrarily large K, it is interesting to note that if one could use $K >> L$ without violating the time-invariance assumption, the bandwidth efficiency of the present implementation would be on the order of (K/L) symbols/second/Hz. Time variation, however, has to be taken into account, and if one were to offer a rule of thumb for the maximal number of transmitters, for the processing scheme used this could be $M_T < \beta K/BT_g$, where $\beta < 1$ is an environmental factor whose value should be decreased as the conditions worsen.

Environmental correlation

Variation in performance over the course of the experiment is quite obvious, and can be as large as several dB from one day to another, or even within a day. This naturally raises the question of performance dependence on the environmental conditions, such as wind and waves. Shown together in figure 7.12 are the joint plots of wave height with the MSE for the SIMO case. Clearly, there exists a correlation with increased MSE during the periods of high waves (which are in turn correlated with high wind speeds).
Other kinds of weather conditions can also be compared, like wave period and wind speed, showing also correlation. This lies on the fact that these magnitudes are indeed correlated with wave height, since strong winds generate strong waves and long wave periods are more likely to be observed when waves are higher. Thus, if the three magnitudes are correlated, they will be also correlated with the MSE along the days of the experiment.

7.2 ICI Compensation

In light of the experimental data, the first question that arises is whether significant ICI exists at all. To answer this question, we look at the autocorrelation of the post-FFT signal. Figure 7.13 illustrates the magnitude of the autocorrelation function

$$R_y(m, n) = \sum_k y_{k+m}(n) y_k^*(n) \tag{7.4}$$

Clearly, there exists strong correlation peaks at lag m=1,2; with another peak at m=20. These peaks indicate the presence of ICI, and motivate testing of ICI suppression methods.

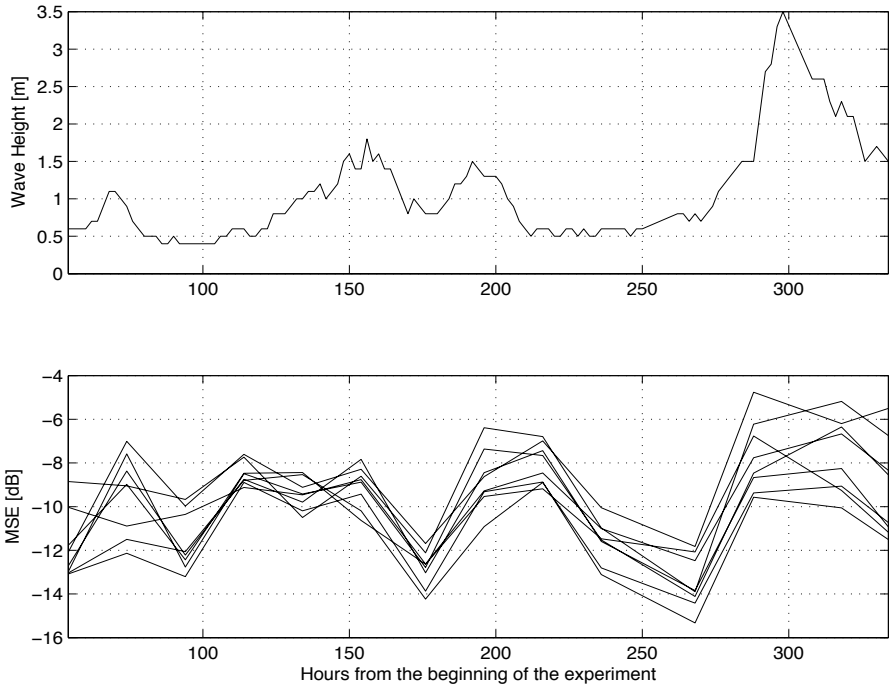

Figure 7.12: Wave height for the days of the experiment (top) and MSE (single transmitter, QPSK and 8-PSK, K=128, 256, 512, 1024).

Ina more detailed manner, the autocorrelation function in equation (7.4) is written, when coupled with equation (2.10):

$$R_y(m,n) = \sum_k \left\{ \sum_{l=0}^{K-1} H_{l,k+m}(n) d_l(n) + w_{k+m}(n) \right\} \left\{ \sum_{i=0}^{K-1} H_{i,k}(n) d_i(n) + w_i(n) \right\}^* \quad (7.5)$$

Considering that the noise is uncorrelated with the signal, the cross products can be eliminated, leading to

$$\begin{aligned} R_y(m,n) &= \textstyle\sum_k \left\{ \sum_{l=0}^{K-1} H_{l,k+m}(n) d_l(n)(n) \right\} \left\{ \sum_{i=0}^{K-1} H_{i,k}(n) d_i(n) \right\}^* + R_n(m,n) \quad (7.6) \\ &= \textstyle\sum_k \sum_{l=0}^{K-1} \sum_{i=0}^{K-1} H_{l,k+m}(n) d_l(n)(n) H^*_{i,k}(n) d^*_i(n) + R_n(m,n) \quad (7.7) \end{aligned}$$

Where $R_n(m,n)$ is the autocorrelation function for the noise post-FFT. Now, using the fact that the $E\{d_l(n)d_i^*(n)\} = \delta i, k$, then the previous expression reduces to

$$R_y(m,n) = \sum_k \sum_{l=0}^{K-1} H_{l,k+m} H^*_{l,k} + R_n(m,n) \quad (7.8)$$

Now, it can be clearly seen that the function $R_y(m,n)$ shows a qualitative measure of the ICI influence. Ideally, if no ICI were present on the system, $H_{l,k+m} = 0$ when $m = 0$ and the autocorrelation function will be a delta. Because this is not the case, peaks at other values than $m = 0$ will be observed.

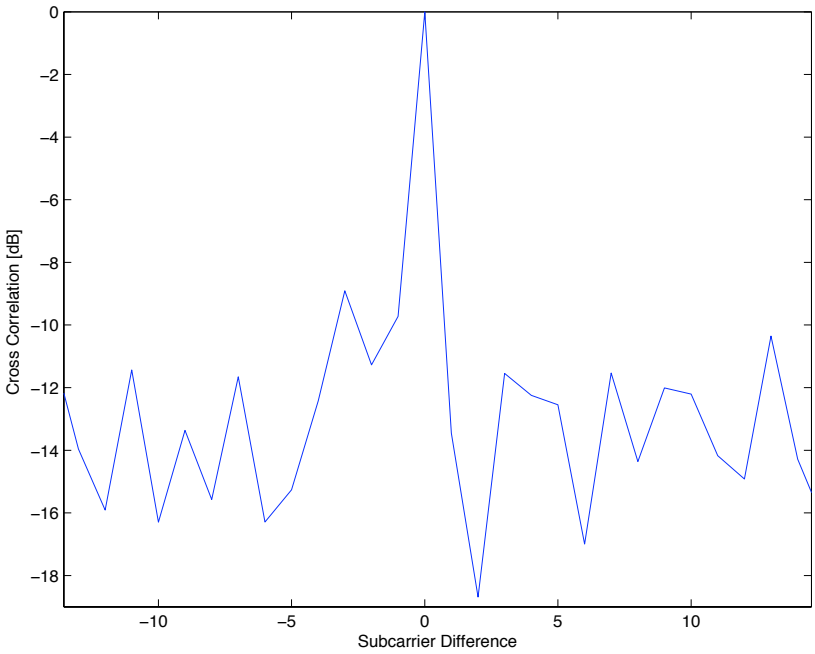

Figure 7.13: Autocorrlation of a received signal (QPSK, $K = 1024$) after FFT demodulation.

Taylor approximation

Figure 7.14 illustrates the performance of this algorithm on an experimental data set. After estimating the channel, a linear equalizer is built using a varying number I of ICI coefficients, as before. The performance of this scheme is very good with a single ICI coefficient, yielding a 1-5 dB improvement at very low computational complexity and little overhead (only the first block is used for training and no pilots after that were used). Other I were tried, leading to similar performance. Obviously I has to be kept as small as possible because of computational expenses. Furthermore, keeping I low eliminates the noise variance which is also contained in the estimated channel matrix. Like in channel sparsing, if the power of the noise is known, the coefficients could be cut off at a certain threshold.
It is important to notice, that this design, although very simple, lead to good improvements. Hence, this result demonstrates that a careful receiver design, which respects the underlying physical processes, can be used to significantly improve the performance, thus pushing the limits on the data rate supported by the band-limited acoustic channel.

Compensation on SIMO systems

In a multichannel receiver, an ICI equalizer is associated with each receiving element. The equalizer corresponding to the r-th receiving element utilizes channel coefficients $\hat{H}^r_{k,l}(n)$, resulting in a set of (preliminary) data symbol estimates, $\hat{d}^r_k(n)$, one for each receiving element $r = 1, \ldots M_R$ life shown in figure 7.15. The data estimates are obtained using

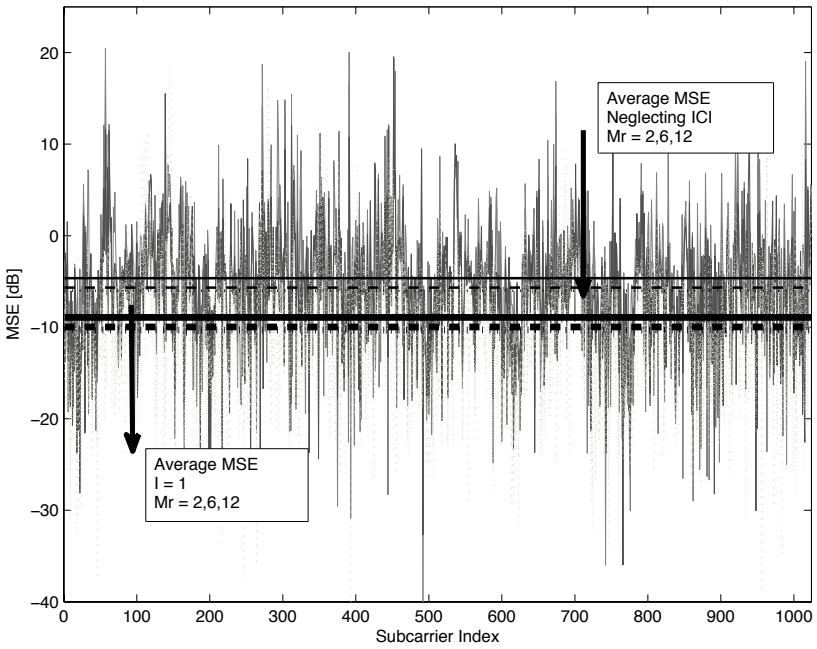

Figure 7.14: Performance of ICI suppression on a QPSK signal set: linear equalization and time-domain channel estimation based on Taylor series model are used. The background light-grey curve corresponds to the ICI equalizer MSE.

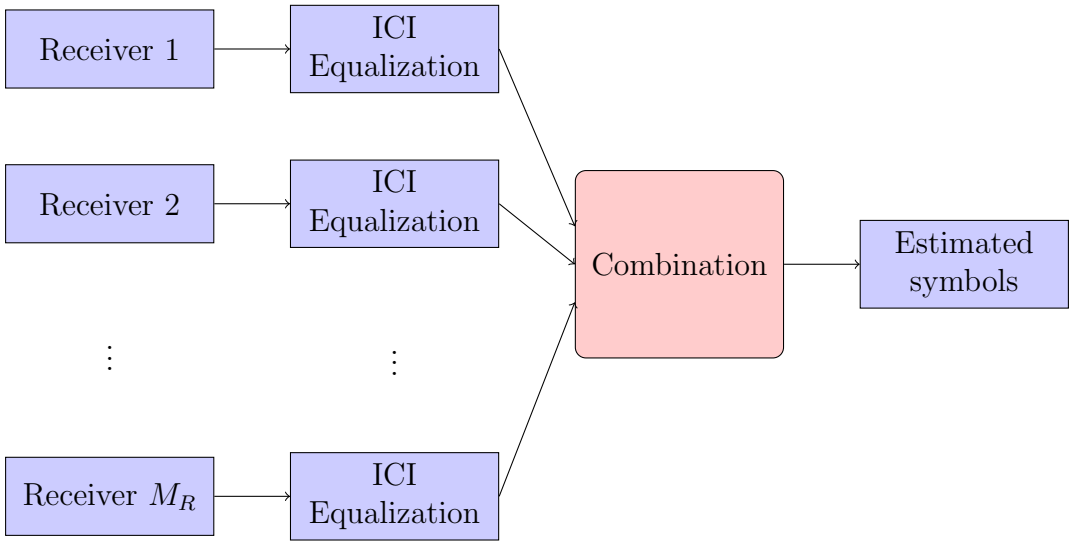

Figure 7.15: Scheme of ICI equalization prior to receiver combination

expression (6.27), after which they are combined to yield the final estimate

$$\hat{d}_k(n) = \sum_{r=1}^{M_R} c_k^r(n)\hat{d}_k^r(n) \tag{7.9}$$

Assuming that the channel estimates are correct, we have that $\hat{d}_k^r(n) = d_k(n) + \nu_k(n)$, where $\nu_k^r(n)$ is the noise. This noise is correlated, both across the carriers and across the

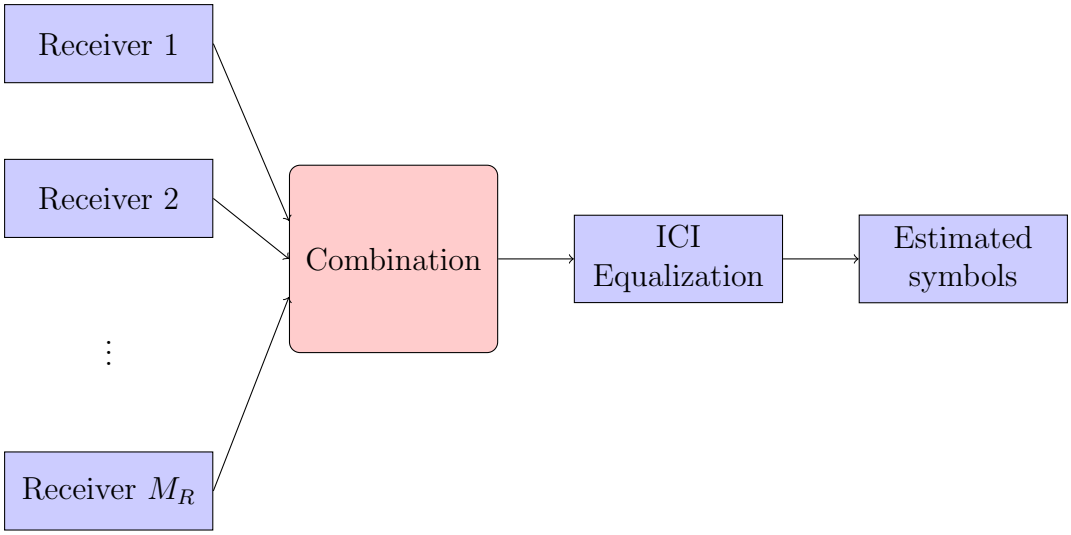

Figure 7.16: Scheme of receiver combination before ICI suppression

receiving elements. The combiner ignores the former in favor of computational complexity, but the latter can be accounted for via maximum ratio combining (MRC). However, to do so, one would need to know the variance of the input noise $w_k^r(n)$. A simpler approach is to perform equal-gain combining (EGC), i.e. to set the combiner weights to $c_k^r(n) = 1$. Although it may seem that combining and equalization are decoupled in this simple approach, we note that tentative symbol decisions used for ICI coefficient estimation are the ones obtained *after* combining; hence, there is a feedback by which the multichannel gain contributes to reliability.
An alternate scheme for ICI suppression would be to perform firstly the combination of the M_R receivers and then perform an ICI cancellation algorithm. This scheme is presented in figure 7.16. Although the optimal system design would be to equalize jointly the ICI using spatial diversity, these methods offer good improvement while keeping the complexity of the system at a reasonable level. ICI equalization obviously offers a significant additional gain. The gain is evident even in the SISO case (M_R =1), although it is modest for the poor-quality data set at hand. As the number of receivers increases, so does the gain of the multichannel equalizer. With 2, 3, and 4 receivers, ICI equalization gains additional 3, 4 and 6 dB, approximately. By increasing the number of receivers beyond 5, the performance saturates with a gain of about 7 dB. Compared with the ICI-neglecting MRC [1], this is a gain of about 1 dB, figure 7.18.
A close analysis to figure 7.18 reveal that an EGC combination performing independent ICI equalization on all the receivers is very close to the optimal MRC combination neglecting ICI. That is to say, if a more careful combination of the receivers could be done, results would probably even show better improvement. Nevertheless, we know that demodulation without compensating this effect is possible, so the system should not be affected by severe ICI and then an improvement on 1dB using all the diversity gain is a good result.

The absolute level of the MSE is also worth noting. This level is directly correlated with the BER performance, and it needs to be above a certain threshold in order for the receiver to operate in a decision-directed mode. While the BER attained at an MSE of -1 dB is often insufcient, an MSE of -5 dB is certainly low enough to provide an open eye

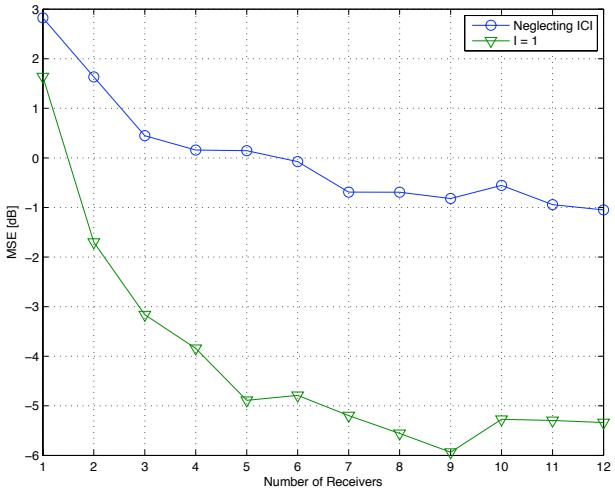

Figure 7.17: Performance of ICI suppression on a SIMO system with a variable number of receivers with EGC.

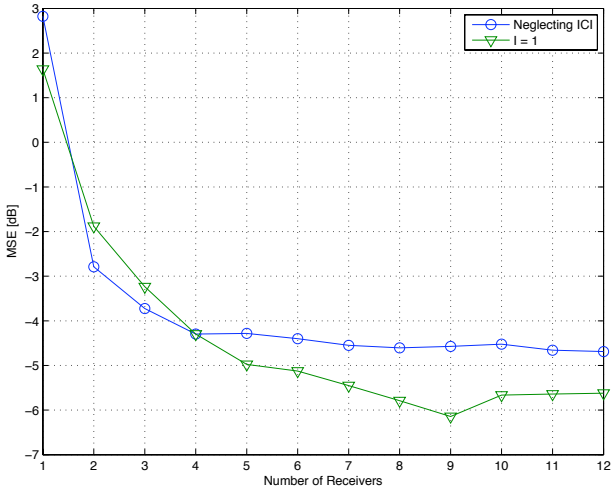

Figure 7.18: Performance of ICI suppression on a SIMO system with a variable number of receivers with MRC.

for the decoder.

Chapter 8

Conclusions

An experimental analysis was conducted to assess the performance and establish the limits of OFDM, a modulation method that offers low-complexity solutions to high-rate communications over band-limited acoustic channels. Two parameters that are key to achieving high bandwidth efficiency in an OFDM system– the number of transmit elements M_T and the number of subcarriers K–were the focal point of experimentation, which included signal processing using (a) MIMO system configurations to support spatial multiplexing of M_T parallel data streams, and (b) ICI equalization to support an increase in K beyond the limit where the time-variation of the channel can be neglected.

Experimental results, obtained with signals recorded in shallow water over the course of two weeks, show variation in performance that can be correlated with the weather conditions, i.e. the wind speed, wave height and wave period. The data set at hand demonstrates the possibility to use two transmit elements, thus doubling the bit rate, while using K=1024 carriers. This "win-win" situation owes to decision-directed adaptive channel estimation and sparsing. Further increase in M_T leads to loss in performance.

The possibility to use large values of K rests on the system's ability to cope with the ICI. Experimental signals were processed using linear equalization in the frequency domain. The equalizer weights are calculated from the ICI coefficients, which are estimated using one of two algorithms: a recursive gradient search in the frequency domain, and an algorithm based on linear modeling of the underlying time-variation. Both techniques demonstrated performance gains, thus indicating the possibility to furhter push the OFDM performance limits.

Future research should concentrate on techniques for ICI equalization, as well as on coupling ICI equalization with MIMO detection.

Bibliography

[1] M. Stojanovic, "Low complexity OFDM detector for underwater acoustic channels," *OCEANS 2006*, pp. 1–6, Sept. 2006.

[2] ——, "Adaptive channel estimation for underwater acoustic MIMO OFDM systems," *Digital Signal Processing Workshop and 5th IEEE Signal Processing Education Workshop, 2009. DSP/SPE 2009. IEEE 13th*, pp. 132–137, Jan. 2009.

[3] M. Stojanovic and J. Preisig, "Underwater acoustic communication channels: Propagation models and statistical characterization," *Communications Magazine, IEEE*, vol. 47, no. 1, pp. 84–89, January 2009.

[4] B. Li, S. Zhou, M. Stojanovic, L. Freitag, and P. Willett, "Multicarrier communication over underwater acoustic channels with nonuniform Doppler shifts," *Oceanic Engineering, IEEE Journal of*, vol. 33, no. 2, pp. 198–209, April 2008.

[5] B. Muquet, Z. Wang, G. Giannakis, M. de Courville, and P. Duhamel, "Cyclic prefixing or zero padding for wireless multicarrier transmissions?" *Communications, IEEE Transactions on*, vol. 50, no. 12, pp. 2136–2148, Dec 2002.

[6] X. Cai and G. Giannakis, "Bounding performance and suppressing intercarrier interference in wireless mobile OFDM," *Communications, IEEE Transactions on*, vol. 51, no. 12, pp. 2047–2056, Dec. 2003.

[7] T. Wang, J. Proakis, and J. Zeidler, "Techniques for suppression of intercarrier interference in OFDM systems," *Wireless Communications and Networking Conference, 2005 IEEE*, vol. 1, pp. 39–44 Vol. 1, March 2005.

[8] A. Gorokhov and J.-P. Linnartz, "Robust OFDM receivers for dispersive time varying channels: equalisation and channel acquisition," *Communications, 2002. ICC 2002. IEEE International Conference on*, vol. 1, pp. 470–474, 2002.

[9] X. Huang and H.-C. Wu, "Robust and efficient intercarrier interference mitigation for OFDM systems in time-varying fading channels," *Vehicular Technology, IEEE Transactions on*, vol. 56, no. 5, pp. 2517–2528, Sept. 2007.

[10] L. Rugini, P. Banelli, and G. Leus, "Simple equalization of time-varying channels for OFDM," *Communications Letters, IEEE*, vol. 9, no. 7, pp. 619–621, July 2005.

[11] K. Tu, D. Fertonani, T. M. Duman, and P. Hursky, "Mitigation of intercarrier interference in OFDM systems over underwater acoustic channels," *IEEE Oceans 2009, Bremen, Germany*, May 2009.

[12] G. Li, H. Yang, L. Cai, and L. Gui, "A low-complexity equalization technique for OFDM system in time-variant multipath channels," *Vehicular Technology Conference, 2003. VTC 2003-Fall. 2003 IEEE 58th*, vol. 4, pp. 2466–2470 Vol.4, Oct. 2003.

[13] T. Kang and R. Litis, "Matching pursuits channel estimation for an underwater acoustic OFDM modem," in *Acoustics, Speech and Signal Processing, 2008. ICASSP 2008. IEEE International Conference on*, 31 2008-April 4 2008, pp. 5296–5299.

[14] S. Mason, C. Berger, S. Zhou, K. Ball, L. Freitag, and P. Willett, "An OFDM design for underwater acoustic channels with Doppler spread," in *Digital Signal Processing Workshop and 5th IEEE Signal Processing Education Workshop, 2009. DSP/SPE 2009. IEEE 13th*, Jan. 2009, pp. 138–143.

[15] G. Taubock, M. Hampejs, G. Matz, F. Hlawatsch, and K. Grochenig, "Lsqr-based ici equalization for multicarrier communications in strongly dispersive and highly mobile environments," in *Signal Processing Advances in Wireless Communications, 2007. SPAWC 2007. IEEE 8th Workshop on*, June 2007, pp. 1–5.

[16] T. Hrycak and G. Matz, "Low-complexity time-domain ici equalization for ofdm communications over rapidly varying channels," in *Signals, Systems and Computers, 2006. ACSSC '06. Fortieth Asilomar Conference on*, 29 2006-Nov. 1 2006, pp. 1767–1771.